DTIC FILE COPY

POR-2227(EX)
(WT-2227)(EX)
EXTRACTED VERSION

OPERATION SUNBEAM, SHOT SMALL BOY

Project Officer's Report

Project 6.2—Magnetic Loop Measurements

P. A. Caldwell, Project Officer
F. N. Wimenitz
J. C. Hoadley
J. S. Wicklund
Harry Diamond Laboratories
Washington, DC

DTIC
ELECTE
JUN 0 2 1987
S D
D

AD-A995 483

26 February 1965

NOTICE:
This is an extracted version of POR-2227 (WT-2227), OPERATION SUNBEAM, Shot Small Boy, Project 6.2.

Approved for public release;
distribution is unlimited.

Extracted version prepared for
Director
DEFENSE NUCLEAR AGENCY
Washington, DC 20305-1000

1 September 1985

87

Destroy this report when it is no longer needed. Do not return to sender.

PLEASE NOTIFY THE DEFENSE NUCLEAR AGENCY ATTN: TITL, WASHINGTON, DC 20305 1000, IF YOUR ADDRESS IS INCORRECT, IF YOU WISH IT DELETED FROM THE DISTRIBUTION LIST, OR IF THE ADDRESSEE IS NO LONGER EMPLOYED BY YOUR ORGANIZATION.

DNA PRINTING PLANT

UNCLASSIFIED
SECURITY CLASSIFICATION OF THIS PAGE

AD-A995-423

REPORT DOCUMENTATION PAGE

1a. REPORT SECURITY CLASSIFICATION UNCLASSIFIED	1b. RESTRICTIVE MARKINGS
2a. SECURITY CLASSIFICATION AUTHORITY	3. DISTRIBUTION/AVAILABILITY OF REPORT Approved for public release; distribution is unlimited.
2b. DECLASSIFICATION/DOWNGRADING SCHEDULE	
4. PERFORMING ORGANIZATION REPORT NUMBER(S)	5. MONITORING ORGANIZATION REPORT NUMBER(S) POR-2227 (EX) (WT-2227) (EX)
6a. NAME OF PERFORMING ORGANIZATION Harry Diamond Laboratories 6b. OFFICE SYMBOL (If applicable)	7a. NAME OF MONITORING ORGANIZATION Defense Atomic Support Agency
6c. ADDRESS (City, State, and ZIP Code) Washington, DC	7b. ADDRESS (City, State, and ZIP Code) Washington, DC
8a. NAME OF FUNDING/SPONSORING ORGANIZATION 8b. OFFICE SYMBOL (If applicable)	9. PROCUREMENT INSTRUMENT IDENTIFICATION NUMBER
8c. ADDRESS (City, State, and ZIP Code)	10. SOURCE OF FUNDING NUMBERS PROGRAM ELEMENT NO. / PROJECT NO. / TASK NO. / WORK UNIT ACCESSION NO.

11. TITLE (Include Security Classification) OPERATION SUN BEAM; SHOT SMALL BOY; PROJECT OFFICER'S REPORT; PROJECT 6.2 - Magnetic Loop Measurements, Extracted Version

12. PERSONAL AUTHOR(S)
P. A. Caldwell, F. N. Wimenitz, J. Carlisle Hoadley, and J. S. Wicklund

13a. TYPE OF REPORT	13b. TIME COVERED FROM ____ TO ____	14. DATE OF REPORT (Year, Month, Day)	15. PAGE COUNT
		650226	117

16. SUPPLEMENTARY NOTATION This report has had sensitive military information removed in order to provide an unclassified version for unlimited distribution. The work was performed by the Defense Nuclear Agency in support of the DoD Nuclear Test Personnel Review Program.

17. COSATI CODES			18. SUBJECT TERMS (Continue on reverse if necessary and identify by block number)
FIELD	GROUP	SUB-GROUP	
8	3		Sun Beam
20	3		Small Boy
			Magnetic Fields

19. ABSTRACT (Continue on reverse if necessary and identify by block number)

The objective of this test was to measure, as a function of time, three mutually perpendicular components of the magnetic component of the electromagnetic field generated by a nuclear detonation. The measurement was to provide values of the field strength in support of theoretical calculations on the mechanism of field generation so as to permit extrapolation to other yields and distances.

The integrated output of three mutually perpendicular loop antennas was recorded on wide-band, self-powered magnetic tape recorders placed at various distances along three different radii from ground zero.

The magnetic field appears to be mainly azimuthal and directed clockwise around ground zero. Although apparent fields were measured in the vertical and radial directions at all stations, they were much smaller than the azimuthal field and were attributed to either local field

20. DISTRIBUTION/AVAILABILITY OF ABSTRACT ☒ UNCLASSIFIED/UNLIMITED ☐ SAME AS RPT. ☐ DTIC USERS	21. ABSTRACT SECURITY CLASSIFICATION UNCLASSIFIED
22a. NAME OF RESPONSIBLE INDIVIDUAL MARK D. FLOHR	22b. TELEPHONE (Include Area Code) 202-325-7559 / 22c. OFFICE SYMBOL DNA/ISCM

DD FORM 1473, 84 MAR — 83 APR edition may be used until exhausted. All other editions are obsolete.

SECURITY CLASSIFICATION OF THIS PAGE
UNCLASSIFIED

FOREWORD

Classified material has been removed in order to make the information available on an unclassified, open publication basis, to any interested parties. The effort to declassify this report has been accomplished specifically to support the Department of Defense Nuclear Test Personnel Review (NTPR) Program. The objective is to facilitate studies of the low levels of radiation received by some individuals during the atmospheric nuclear test program by making as much information as possible available to all interested parties.

The material which has been deleted is either currently classified as Restricted Data or Formerly Restricted Data under the provisions of the Atomic Energy Act of 1954 (as amended), or is National Security Information, or has been determined to be critical military information which could reveal system or equipment vulnerabilities and is, therefore, not appropriate for open publication.

The Defense Nuclear Agency (DNA) believes that though all classified material has been deleted, the report accurately portrays the contents of the original. DNA also believes that the deleted material is of little or no significance to studies into the amounts, or types, of radiation received by any individuals during the atmospheric nuclear test program.

QUALITY INSPECTED 1

Accesion For	
NTIS CRA&I	☑
DTIC TAB	☐
Unannounced	☐
Justification	
By	
Distribution /	
Availability Codes	
Dist	Avail and / or Special
A-1	

UNANNOUNCED

OPERATION SUN BEAM

SHOT SMALL BOY

PROJECT OFFICERS REPORT—PROJECT 6.2

MAGNETIC LOOP MEASUREMENTS

Paul A. Caldwell
Project Officer
Francis N. Wimenitz
J. Carlisle Hoadley
John S. Wicklund

Harry Diamond Laboratories
Washington, D. C.

This document is the author(s) report to the Director, Defense Atomic Support Agency, of the results of experimentation sponsored by that agency during nuclear weapons effects testing. The results and findings in this report are those of the author(s) and not necessarily those of the DOD. Accordingly, reference to this material must credit the author(s). This report is the property of the Department of Defense and, as such, may be reclassified or withdrawn from circulation as appropriate by the Defense Atomic Support Agency.

DEPARTMENT OF DEFENSE
WASHINGTON, D.C. 20301

ABSTRACT

This experiment was performed to measure the magnetic field component emanating from a nuclear device. The measurements were made in an attempt to clarify the mechanisms of generation of electromagnetic field.

The integrated output of three mutually perpendicular loop antennas was recorded on wide-band, self-powered magnetic tape recorders placed at various distances along three different radii from ground zero.

The magnetic field appears to be mainly azimuthal and directed clockwise around ground zero. Due to instrumentation difficulties in most cases, no reliable information in the first 10 μsec was recorded; however, the later portions of the signals correlate well with present theories.

Although apparent fields were measured in the vertical and radial directions at all stations, they were much smaller than the azimuthal field and were attributed to either local field distortions or antenna misalignment.

A vertical magnetic signal attributable to the expulsion of the earth's magnetic field was measured at the 250-foot station.

At the 625- and 1,600-foot stations, a close correlation between the shape of the azimuthal magnetic field and the gamma ray time history curves was found.

Measurements at 1,600 feet and the 100-foot depth indicate that the wave shape of the azimuthal field is determined more by the transmission medium than by the source.

CONTENTS

ABSTRACT ---------- 5

CHAPTER 1 INTRODUCTION ---------- 9

1.1 Objectives ---------- 9
1.2 Background ---------- 10
1.3 Theory ---------- 10

CHAPTER 2 PROCEDURE ---------- 13

2.1 Field Installations ---------- 13
2.2 Recorder Magnetic Shield ---------- 14
2.3 Antenna System ---------- 14
2.4 Calibration of Loop Antennas ---------- 22
2.5 Recording System ---------- 28
2.5.1 Design ---------- 29
2.5.2 Magnetic Recording Heads ---------- 30
2.5.3 Tape Transport ---------- 33
2.5.4 Integrators ---------- 35
2.5.5 Voltage Controlled Oscillator ---------- 40
2.5.6 Record Amplifier ---------- 43
2.5.7 Fiducial Markers ---------- 46
2.5.8 Timing Oscillator ---------- 51
2.5.9 Fiducial Mixer ---------- 53
2.5.10 Patch Cards ---------- 55
2.5.11 Automatic Sequencing System ---------- 56
2.6 Playback System ---------- 58
2.7 System Calibration ---------- 59

CHAPTER 3 RESULTS ---------- 80

3.1 Data Analysis ---------- 80
3.2 Data ---------- 81
3.2.1 Azimuthal Field ---------- 82
3.2.2 Vertical and Radial Fields ---------- 84
3.2.3 Shock Arrival Measurements ---------- 86

CHAPTER 4 CONCLUSIONS AND RECOMMENDATIONS ---------- 115

REFERENCES ---------- 116

TABLES

2.2 Project 6.2 Station Locations ---------- 61
2.3 Electronic Recorder Assembly Operation Sequence ---------- 62
2.4 Integrator Rate Gain and Decay Times ---------- 63
2.5 Fluor to Detector Distances and Aperture Sizes ---------- 64
2.6 Detector-Mounting-Tube Temperature Measurements ---------- 64

FIGURES

2.1 Project 6.2 pit station diagram ---------- 65
2.2 Project 6.2 station locations ---------- 66
2.3 Equivalent circuits for a shielded loop antenna ---------- 67
2.4 Calibration of antenna ---------- 68
2.5 Experimental arrangement for calibration of antennas ---------- 69
2.6 Block diagram HDL SB 1 recorder ---------- 70
2.7 Small Boy recorder open for servicing ---------- 71
2.8 Conceptual diagram of integrator ---------- 72
2.9 P65 integrator schematic ---------- 73
2.10 Rixon integrator schematic ---------- 74
2.11 Record amplifier schematic ---------- 75
2.12 Teller light fiducial marker ---------- 76
2.13 Timing oscillator schematic ---------- 77
2.14 Fiducial mixer schematic ---------- 78
2.15 Patch card schematic ---------- 79
3.1 Typical uncorrected magnetic field oscillograph ---------- 87
3.2 Azimuthal magnetic field, Station 519.01, 250-foot ground range ---------- 88
3.3 Azimuthal magnetic field, Station 519.02, 625-foot ground range ---------- 89
3.4 Azimuthal magnetic field, Station 519.09, 625-foot ground range ---------- 90
3.5 Azimuthal magnetic field, Station 519.10, 1,600-foot ground range ---------- 91
3.6 Azimuthal magnetic field, Station 519.08, 1,600-foot ground range ---------- 92
3.7 Azimuthal magnetic field, Station 519.06, 4,000-foot ground range ---------- 93
3.8 Azimuthal magnetic field, Station 519.11, 4,000-foot ground range ---------- 94
3.9 Azimuthal magnetic field, Station 519.07, 9,800-foot ground range ---------- 95
3.10 Azimuthal magnetic field, Station 519.05, 100-foot depth, 1,600-foot ground range ---------- 96
3.11 Comparison azimuthal magnetic field with radiation detector current, 625-foot ground range ---------- 97
3.12 Comparison azimuthal magnetic field with radiation detector current, 1,600-foot ground range ---------- 98
3.13 Vertical magnetic field, Station 519.01, 250-foot ground range ---------- 99
3.14 Vertical magnetic field, Station 519.02, 625-foot ground range ---------- 100
3.15 Vertical magnetic field, Station 519.09, 625-foot ground range ---------- 101
3.16 Vertical magnetic field, Station 519.10, 1,600-foot ground range ---------- 102
3.17 Vertical magnetic field, Station 519.08, 1,600-foot ground range ---------- 103
3.18 Vertical magnetic field, Station 519.06, 4,000-foot ground range ---------- 104
3.19 Vertical magnetic field, Station 519.11, 4,000-foot ground range ---------- 105
3.20 Vertical magnetic field, Station 519.07, 9,800-foot ground range ---------- 106
3.21 Vertical magnetic field, Station 519.05, 100-foot depth, 1,600-foot ground range ---------- 107
3.22 Radial magnetic field, Station 519.09, 625-foot ground range ---------- 108
3.23 Radial magnetic field, Station 519.10, 1,600-foot ground range ---------- 109
3.24 Radial magnetic field, Station 519.08, 1,600-foot ground range ---------- 110
3.25 Radial magnetic field, Station 519.06, 4,000-foot ground range ---------- 111
3.26 Radial magnetic field, Station 519.10, 4,000-foot ground range ---------- 112
3.27 Radial magnetic field, Station 519.07, 9,800-foot ground range ---------- 113
3.28 Radial magnetic field, Station 519.05, 100-foot depth, 1,600-foot ground range ---------- 114

CHAPTER 1

INTRODUCTION

1.1 OBJECTIVES

The objective of the test was to measure, as a function of time, three mutually perpendicular components of the magnetic component of the electromagnetic field generated by a nuclear detonation. The measurement was to provide values of the field strength in support of theoretical calculations on the mechanism of field generation so as to permit extrapolation to other yields and distances.

In order to adequately satisfy this requirement, data were required: (1) along a radial line at several distances from ground zero (starting at no less than 100 m and out to at least 3 km), (2) with a combined systems rise time of approximately 1 μsec and out to at least 1 second (10 seconds desired), (3) along at least two geomagnetic directions, (4) at a depth of at least 100 feet at one distance, (5) at a height of at least 20 feet above the surface for one field component at one distance.

Correlation of the magnetic field data in real time with good geometry gamma flux measurements was desired. The total gamma flux (poor geometry) at the loops was to be measured at some of the stations for an evaluation of ionization density and

other parameters on the same time base.

1.2 BACKGROUND

This project was a follow-up of Project 6.2 of Operation Plumbbob where essentially the same parameters were measured over a variety of yields but with somewhat less sophisticated instrumentation. Although the results of this project (Reference 1) constituted the only available near field data, there was insufficient quantity of useful points for any one yield, orientation, and weapon design and experimental configuration to allow the establishment of firm yield-range scaling laws.

The data were required for a determination of the extent of electromagnetic disturbances induced in electronic circuits and communication cables associated with installations hardened against the effect of blast, shock, and thermal radiation. Underground missile launching sites are examples of such installations.

1.3 THEORY

Present uncertainties in the theoretical discussions are such that nothing would be served by a discussion of any of the theories presented to date. Reference 2 contains a discussion of present theories and Reference 3 presents an extensive bibliography of reports.

In the meantime, the empirical scaling laws derived in Reference 1 were used to predict values for the azimuthal field H_ϕ which were to be expected. The values of field are given by the equation

$$H_\phi = - \frac{1.8 \times 10^7 \, Y^{0.5}}{R^2} \quad \text{Amp turns/meter}$$

where Y is the yield in kilotons and R the slant range in meters. Alternatively, an equation derived by Longmire

$$H_\phi \simeq 8 \times 10^3 \left[\frac{W_e}{R^2} \exp(-R/0.4)\right]^{0.45} \quad \text{Amp turns/meter}$$

where W is the yield in megatons and R is the distance in kilometers, predicts field values which differ at most by a factor of ten at distances of the order of 500 meters and agrees quite closely with the values of Reference 1 at both smaller and larger distances (see Figure 1.1). There still appears to be considerable disagreement regarding the origin of the vertical and radial field H_z and H_r. If these fields are indeed, as is presently thought by some theoreticians, simply the effect of field tilting from ground inhomogeneities, then there is no simple way of predicting their values. It appears that the empirical scaling laws of Reference 1 provided the best available forecast for expected field strengths.

Page 12 is deleted

CHAPTER 2

PROCEDURE

2.1 FIELD INSTALLATIONS

In order to protect the recorders from blast, shock, and nuclear radiation, they were suspended on springs at the bottom of unreinforced concrete pits, which were capped with concrete plugs. The thickness of the concrete in the walls and plugs was determined by the distance from ground zero. See Figure 2.1 for details. Sufficient concrete was used so as not only to make the pit invulnerable to the effects of shock and blast, but also to provide sufficient shielding from neutron and gamma rays to reduce the gamma flux at the surface of the recorder to less than 10^4 r/sec and to reduce the neutron dose to less than 10^9 n/cm^2. Table 2.1 shows a comparison of radiation measurements made during the shot on the surface of the various stations with those made inside the recorders.

In order to accomplish the aims of the experiment, eleven locations were used as shown in Figure 2.2. The ground range for each station is given in Table 2.2.

The purpose of the stations on the line N43°E was to obtain scaling laws for distance, evaluate relations to obtain scaling laws for distance, evaluate relations to the Malik sphere radius, gamma mean free path, etc. The stations on

the N17°W line were to assess possible east-west effects from interaction with the earth's magnetic field. The 100-foot-deep station at 1,600 feet was to assess field and/or current penetration into the ground and to provide data for possible mechanisms of earth field displacement. The three closest stations were located inside the ionized sphere radius and the last was outside the sphere. Those stations at 4,000 feet were on the fringe. Station 519.08 was to provide data for the more realistic case where cables cover the ground surface, as well as provide field data for the current measurements in that area. Station 519.03 was to provide the loop measurement at a height of 20 feet.

2.2 RECORDER MAGNETIC SHIELD

The magnetic shield boxes were similar to the ones used in Operation Plumbbob and described in Reference 1. They consisted of a 1/8-inch SAE 10-10 steel outer shield and two insulated 0.025-inch Mu-metal shields. Calculations indicated that the composite shield would attenuate a signal by a factor of about 3×10^9.

2.3 ANTENNA SYSTEM

The antennas used were similar to those used in Operation Plumbbob (Reference 1) to measure close-in magnetic fields.

The antennas were arranged at each station in three mutually perpendicular axes and oriented in such a way that a positive H_z, the vertical component, is directed up from the ground plane; a positive H_r, radial component, is directed out from ground zero; a positive H_ϕ, azimuthal component, is directed counter-clockwise around ground zero.

The significant parameters of the loop antenna were determined by procedures described below.

The equivalent circuit for the shielded loop antenna was taken from Reference 5 and is shown in Figure 2.3a.

The left half of the circuit refers to the shield. C_1 and R_1 are the capacitance and resistance of the gap and L_1 is the inductance of the shield. The emf (electromotive force) induced in the shield by the changing magnetic field is represented by e_1 and is proportional to the rate of change of the magnetic flux density.

The right half of the circuit in Figure 2.3a represents the loop proper. L_2 is its inductance, C_2 its distributed capacitance, and R_2 is the resistance between terminals (the series resistance of the wire itself is small enough to be negligible in this case). The emf e_2 is that induced in the loop by the changing magnetic field. Since the loop is quite symmetrically threaded through the outer shield, it follows that $e_2 = ne_1$, where n is the number of turns in the loop.

The shield and loop are coupled through their mutual inductance, M. The coupling coefficient is defined through the relation $n^2L_1 = k^2L_2$ (or equivalently, $M^2 - k^2L_1L_2$). Perfect coupling corresponds to $k^2 = 1$, which is the case, for all practical purposes, for these particular antennas. Detailed analysis (referred to later) indicates the major effect of imperfect coupling is the appearance of small-amplitude, high-frequency ($\sim 10^8$ cps) oscillations which have not been observed with laboratory apparatus much more sensitive than the recording units used in the field.

Analytical procedures can be used to solve the circuit of Figure 2.3a, but the effort involved is multiplied when a cable with capacitance and inductance (such as was used in the actual measurements) is added. To a good approximation, the equivalent circuit of this configuration is given by Figure 2.3b. Here C_1, R_1, L_1, M, e_1, and e_2 have the same meanings as previously. C_2 now represents the parallel capacitance of the antenna and the cable, L_3 is the cable inductance, and R_2 is now the cable termination. Since the cable termination is only a few hundred ohms, any other dc resistance across the antenna or cable is negligible. It will be seen later that the cable capacitance and inductance can be considered as lumped parameters for this application.

Analytical methods for assessing the relative importance of the various parameters in Figure 2.3b become laborious, resulting in equations which must be solved by numerical methods. Happily, the loop equations of the circuit of Figure 2.3b are easily solved by standard analog computer techniques. Varying the value of a particular component then consists of varying a potentiometer and observing the change in the transfer function by means of an oscilloscopic display.

The analog computer method was verified in two ways. The first was direct comparison with experiments (described later) performed with the actual antennas and cables used in the field. The second was comparison with analytic results for the circuit of Figure 2.3a. In all instances, agreement was excellent and gives a high degree of confidence in the results obtained with the computer.

Among the important results obtained by computer techniques were

1. The resistor R_1 can be taken as infinite. The computer results showed that R_1 could be reduced to a few thousand ohms without affecting the transfer function when R_2 was of the order of a few hundred ohms or less (this was experimentally verified by putting a carbon resistor across

the gap of an actual antenna). For the field measurements, the gaps were filled with potting compound which had an initial resistance of the order of 10^7 ohms. Nothing which is known about the behavior of potting compounds and air under high radiation rates (Reference 2) indicates that R_1 could fall below this few thousand ohms at any time during the detonation.

2. The cable inductance, L_3, can be ignored for the terminating resistance, R_2, used in the measurements. This inductance does not show any appreciable effect until the terminating resistance becomes about 100 ohms or less. Since the results obtained using Figure 2.3b as a model were in excellent agreement with experiment, it then follows that the cable parameters can be considered lumped, rather than distributed,

3. The coupling coefficient k^2 can be considered unity for the measurements taken in the field. When in the analog computer calculation the coupling coefficient was reduced below unity, pronounced (although of relatively small amplitude), high-frequency ($\sim 10^8$ cps) oscillations became manifest, although never important for the actual values of the circuit parameters. The high frequency precludes recording any such oscillations with the equipment used; the low amplitude precludes any

other disturbance from being introduced into the system by this effect. Accordingly, any deficiency in the coupling is manifest only in the sensitivity (determined separately by calibration) and not in the waveshape. Direct measurement of the inductance also showed that the coupling coefficient was very close to unity.

The three factors enumerated above permit the use of the simplified circuit shown in Figure 2.3c.

This simplified circuit is easily analyzed and yields the tranfer function

$$V(s) = \frac{n}{(L_1 C_1 + L_2 C_2) + \frac{L_2}{R_2} S + 1} \qquad (2.1)$$

for the voltage developed across the resistor. The relation $M^2 = L_1 L_2$ was used in the derivation of Equation 2.1, but the relation $n^2 L_1 = L_2$ was explicitly avoided to retain easily-recognizable parameters. The response to a δ-function of

strength E in the time domain, then, is

$$V(t) = Ae^{-at} \sin\omega t, \tag{2.2}$$

where

$$a = \frac{L_2}{2R_2} = \frac{1}{(L_1C_1 + L_2 C_2)} \; ; \quad \omega = \frac{1}{(L_1C_1 + L_2C_2)} - \left[\frac{L_2}{2R_2(L_1C_1 + L_2C_2)} \right]^2$$

and $A = (a^2 + \omega^2)$ nE. The voltage E is, of course, related to the time rate of change of the magnetic field intensity through the loop calibration constant.

The ringing described by Equation 2.2 can be achieved quite easily and the circuit parameters a and ω for any particular antenna-cable-resistor combination can be obtained. In this experiment, a single loop of wire was taped to the loop antenna and a switch connected this wire to a dc power supply (a square wave generator with a long period was also used on occasion). The extremely sharp rise in current in the wire closely approximated a step function. Since the voltage induced in the antenna was proportional to the derivative of this current, a δ-function input was achieved. The constants a and ω for any desired antenna-cable combination were then obtained through analysis of photographs of resultant oscillographic traces. The values so obtained were in excellent agreement with those obtained by direct calculation from measured values of the circuit parameters.

It is noted in passing that the optimum cable termination can be obtained from Equation 2.2. This is not the characteristic impedance of the cable, since the inductance added by the antenna is large compared to that of the length of cable used. Critical damping of Equation 2.2 occurs when $R_2 = \frac{1}{2}\left(\frac{L_2}{\frac{L_1}{L_2}C_1 + C_2}\right)^{1/2}$. Substantiation of the calculated value was obtained by direct experimentation, as well as simulation on the analog computer.

Loop parameters were obtained by Q-meter, Rx meter, and the photographic method described previously. The results were substantially the same. Greater accuracy was achieved by utilizing an extrapolation technique for all methods. In this technique, the resonant frequency of the loop was obtained in the open-circuited condition. Then R_2 in Equation 2.2 is effectively infinite and ω becomes $(L_1C_1 + L_2C_2)^{-1/2}$. Here C_2 is the capacitance of the loop. If an external capacitance C_a is added, $\omega = [L_1C_1 + L_2(C_2 + C_a)]^{-1/2}$. The external capacitance is varied and ω is measured. The quantity $\frac{1}{\omega^2}$ is plotted as a function of frequency and a straight line results. The slope of this line is L_2. Extrapolation to the intercept yields $\frac{L_1}{L_2}C_1 + C_2$. Least squares determinations make this a quite

accurate technique, particularly in the value of the slope. Suitable corrections are made for leads, connectors, etc.

The loop is then removed and the process repeated for the shield alone. Here only L_1 can be obtained by the least squares method, since C_1 is the capacitance of the gap alone while the technique measures distributed capacitance as well. C_1 was obtained by cutting the shield and measuring the capacitance directly.

Values of the loop parameters, then, are:

$L_1 = 0.50\ \mu h$, $C_1 = 25$ pf

$L_2 = 18.0\ \mu h$ $C_2 = 25$ pf

The resonant frequency of the antenna with 30 feet of RG 22 cable calculates to 1.7 megacycles. The average measured values were 1.6 megacycles.

Accuracy of these values is much better than 10 percent, actually approaching 1 percent in the case of the inductance.

2.4 CALIBRATION OF LOOP ANTENNAS

The loop antennas were calibrated in the known field of a large Helmholtz coil. To use oscilloscopic techniques, it was convenient to have the output of the antenna approximate a square pulse. Since the open circuit voltage induced in the

loop antenna is proportional to the time derivative of the current through the Helmholtz coil, a ramp function in voltage was applied across the Helmholtz coil.

The ramp function was produced by a function generator. Were there no inductance in the Helmholtz coil, the current would be a ramp function and the open circuit voltage induced in the antenna would be a square pulse. Due to inductance of the coil, however, rounding of the corners occurs. This rounding can be reduced by introducing a series resistance.

Assume that the capacitance of the Helmholtz coil can be neglected and that the measured voltage across the terminals of the loop antenna is directly proportional to the time derivative of the current in the Helmholtz coil. It can be shown that both assumptions are valid in this case.

If L is the inductance and R the resistance of the Helmholtz coil, then

$$e(t) = L \frac{di}{dt} + Ri$$

describes the current as a function of the input voltage. The response to

$$e(t) = \delta(t) \quad \text{is} \quad i(t) = \frac{1}{L} e^{-\frac{Rt}{L}}$$

so the response to an arbitrary input voltage F(t) is

$$i(t) = \frac{1}{L}\int_0^t e^{-\frac{R}{L}\tau} F(t-\tau)\,d\tau = \frac{e}{L}^{-\frac{R}{L}t}\int_0^t e^{\frac{R}{L}\tau} F(\tau)\,d\tau$$

In this case,

$$F(t) = \frac{V}{T}[t - H(t-T)]$$

where $H(t-T)$ is the unit step function defined by $H(t-T) = 0,\ t < T$; $H(t-T) = 1,\ T \geq t$. It is assumed that the signal begins at $t = 0$. Then

$$i(t) = \frac{V}{LT} e^{-\frac{R}{L}t}\left[\int_0^t d\tau - \int_0^t H(\tau - T)\cdot(\tau - T)\, e^{\frac{R}{L}\tau} d\tau\right]$$

The second integral is non-zero only when $\tau \geq T$ and, therefore, only when $t \geq T$, since the upper limit is t. The step function can then be removed from inside the integral and the lower limit changed to give

$$i(t) = \frac{V}{LT} e^{-\frac{R}{L}t}\left[\int_0^t \tau e^{\frac{R}{L}\tau} d\tau - H(t-T)\int_T^t (\tau - T)\, e^{\frac{R}{L}\tau}\right]$$

$$i(t) = \frac{V}{TR}\left\{ t + \frac{L}{R}\left(e^{-\frac{R}{L}t} - 1\right) - H(t-T)\left[t - T + \frac{L}{R}\left(e^{-\frac{R}{L}(t-T)} - 1\right)\right]\right\}$$

This equation can also be written in the form

$$i(t) = \frac{V}{TR}\left[t + \frac{L}{R}\left(e^{-\frac{R}{L}t} - 1\right)\right],\quad 0 < t < T$$

$$i(t) = \frac{V}{TR}\left[T + \frac{L}{R} e^{-\frac{R}{L}t}\left(1 - e^{\frac{R}{L}T}\right)\right],\quad T < t$$

Since H (t), the magnetic field, near the center of the Helmholtz coil is proportional to i (t), the above is a representation of the field.

It has been assumed that the output of the antenna is proportional to the time derivative of the field; therefore, differentiation of the above equation is valid and yields

$$\frac{di}{dt} = \frac{V}{TR}\{1 - e^{-\frac{R}{L}t} - \delta(t - T)[t - T + \frac{L}{R}(e^{-\frac{R}{L}(t - T)} - 1)]$$

$$- H(t - T)[1 - e^{-\frac{R}{L}(t - T)}]$$

The term with the δ - function is always zero, so

$$\frac{di}{dt} = \frac{V}{TR}\{1 - e^{-\frac{R}{L}t} - H(t - T)[1 - e^{-\frac{R}{L}(t - T)}]\}$$

This equation can be written in the form

$$\frac{di}{dt} = \frac{V}{TR}(1 - e^{-\frac{R}{L}t}), \quad 0 < t < T$$

$$\frac{di}{dt} = \frac{V}{TR} e^{-\frac{R}{L}t}(e^{\frac{R}{L}T} - 1), \quad T < t$$

Examination of the first of the above equations shows that, for given T and L, resistance can be added in series to make di/dt as close to V/TR as desired at time t - T. The resistance

R is then the sum of the resistance of the coil at time $t = T$. The resistance R is then the sum of the resistance of the coil and the series resistor.

If it is required that $\frac{di}{dt}$ rise to within ϵ of the value $\frac{V}{TR}$ in time T,

$$e^{-\frac{R}{L}} < \epsilon$$

whence

$$\frac{R}{L} < -\frac{1}{T} \ln \epsilon$$

For the Helmholtz coil used, L = 60 microhenries, T = 50 microseconds, and the desired accuracy ϵ was 0.1 percent. Then any resistance greater than

$$\frac{6 \times 10^{-5}}{5 \times 10^{-5}} \times 6.91 = 8.3 \text{ ohms}$$

will yield the desired accuracy.

The antenna calibration is determined in the following way. The magnetic field near the midpoint of a Helmholtz coil is given by

$$H = Ki$$

where K is a geometric constant determined in advance either by theory or calibration. The open circuit voltage across the antenna is given by

$$v_{ant} = -k\frac{dH}{dt} = -kK\frac{di}{dt}$$

where k is the desired calibration constant.

The maximum value of $\frac{di}{dt}$ occurs when t = T, at which time the value is $\frac{V}{TR}$ to within the desired accuracy. Thus,

$$v_{max} = -kK\frac{V}{TR}$$

The output of the antenna is displayed on an oscilloscope and the value at maximum is determined.

The antenna constant is then determined from three simple measurements of v_{max}, T, and V.

$$k = \frac{v_{max}T}{V} \cdot \frac{R}{K}$$

where R = resistance in series with the Helmholtz coil equal to 9.86 ohms

K = geometric constant of Helmholtz coil equal to 4.97 turns/meter (see Reference 4)

v_{max} = maximum value of antenna output

V = maximum voltage across series resistance R

T = time in which ramp input current rises from zero to maximum value.

Figure 2.4 shows a typical oscilloscopic display.

Figure 2.5 shows the experimental arrangement for calibration of antennas.

2.5 RECORDING SYSTEM

The recording system, built to HDL (Harry Diamond Laboratories) specifications by the Rixon Electronics Corporation, had a basic recording capability of an information bandwidth extending from dc to over 300 kc on each of fourteen frequency-modulated non-bias recording channels on 1-inch magnetic tape.

Sufficient circuit simplification resulted from the use of nonbias recording and wide-band, wide-deviation FM recording in conjunction with complete circuit transistorization to make it feasible to package the system in a volume only slightly larger than the original Plumbbob recording system. Transistorization of the electronic system eliminated the necessity for motor generators and power transformers, since the transistors' operating potentials could be provided directly by the main battery.

Wide-band recording was accomplished by the ± 30-percent modulation of a 710-kc carrier using an index of less than 1 which results in an intelligence bandwidth extending from dc to over 300 kc.

The FM signal was recorded directly on magnetic tape without using high-frequency bias by an increase in the head current to a value about 10 times the normal signal value which

is usually used for the HF bias itself. Amplitude distortion (in the intelligence signal) was minimized because: (1) the discriminator, which read out the reproduced signal, was not amplitude-sensitive (within limits), and (2) the voltage-controlled oscillator's (VCO) 710-kc carrier frequency served to maintain the magnetic head in the center of its magnetic hysteresis loop operating characteristic.

By operating at this high signal level, saturation recording resulted, which further tended to reduce amplitude variations of the tape.

2.5.1 Design. The recording system consisted of fourteen similar channels of FM recording utilizing plug-in modules which allowed a large degree of flexibility in tailoring each channel to suit input sensor information characteristics.

The basic module sequence was where an input sensor (loop antenna) output was connected to an integrator and then to a VCO, the output of which drove a record amplifier which in turn drove a magnetic record head track.

Twelve information channels were provided plus two channels (one for each magnetic head stack) devoted to a timing oscillator and zero-time fiducial marker (see Figure 2.6).

The recorder package included fourteen identically wired, shielded series of compartments designed to hold fourteen of the basic module sequences. In addition, there were provided three oscillator compartments and two patch card compartments.

The oscillator compartments were wired to allow insertion of two timing oscillator modules and a bias oscillator module. For this program the bias oscillator was not used since the HF bias, which is essential for analog recording, is not necessarily required when FM recording is used.

The twelve integrator compartments (integrators were not used on the timing channels) were symmetrically disposed about two patch card compartments which were wired to integrator compartments to allow plug-in patch cards to establish specific integrator characeristics, insertion of attenuation ahead of the integrators, and the interconnection of any integration input to any input sensor.

The mechanical configuration of the electronic plug-in assembly was arranged so that like functions extended horizontally and tracked identification vertically, as can be seen in the photograph, Figure 2.7.

2.5.2 Magnetic Recording Heads. The heads used in the recorder consisted of two Ampex seven-channel units with

staggered tracks (i.e., head No. 1 contained the odd tracks and head No. 2 the even tracks). The two units were mounted such that the tracks were interleaved with one head stack mounted in advance of the other to result in a 14-track array.

This head configuration, which conformed to IRIG standards, gave rise to timing problems since the recorded signals on half of the channels were displaced along the tape a distance equal to the gap-to-gap spacing of the mounted record head stacks. If the signals were played back on the same heads, i.e., with identical spacing, there would be no problem. This, however, was not the case. Consequently, signals which might have occurred simultaneously when reproduced occurred at different times depending on which track the signal output was being taken from.

Since the delay between head stacks was a fixed quantity, it could be handled by proper calibration in the readout process, but there were other time displacements associated with magnetic heads which were more difficult to handle.

These delays arose from a number of sources including: (1) flutter, (2) gap scatter, and (3) azimuthal scatter.

Flutter. There was a time jitter associated with interleaved head stacks which arose from vibration of the tape between the heads due to variations in tape tension and tape

surface and head surface friction. This resulted in a frequency modulation of the recorded signals at a frequency mainly determined by the physical length of tape between the head gaps. In the present system, this amounted to ± 2.5 μsec jitter.

Gap Scatter. A significant source of delay error was caused by gap scatter, i.e., random displacement of each head gap due to mechanical manufacturing tolerances and in changes which occur to the magnetic characteristics of the core material in the gap area when the head surfaces are finish-lapped. Since the gap spacer thickness was on the order of 125 microinches plus or minus a few microinches, it can be seen that magnetic head mechanical tolerances approached optical wavelengths and were extremely difficult to maintain. Assuming that the heads conformed to the manufacturer's specifications of less than 100 microinch gap-scatter, there would result delays in the order of 1.0 microsecond from this source.

Azimuthal Gap Scatter. This is the angular displacement of the gap of each track from a line drawn through the center of the seven gaps in a stack and is probably associated with non-homogeneous changes in magnetic characteristics of the head material in the core at the gap area during the final lapping process. Azimuthal scatter in terms of an angular displacement

has been measured to be as high as 12-db reduction in reproduced signal output from a tape. This alignment loss is given by:

$$30 \log \frac{\sin \frac{W \tan a}{\lambda}}{\frac{W \tan a}{\lambda}} \text{ db}$$

where W = width of the recorded track = 0.05 inch

a = angle of misalignment

λ = wavelength of recorded signal, inches

The signal loss due to head misalignment was minimized on playback by adjustment of each track for maximum signal output on the tape.

2.5.3 Tape Transport. The function of a tape transport is to cause magnetic tape to be transferred at a constant rate from one reel to another, passing over magnetic recording heads on the way. All design efforts are pointed toward insuring constant tape speed and constant intimate contact between the magnetic surface of the tape and the activated area of the recording head. Accomplishment of these goals requires the maintenance of extreme rigidity between mechanical members, usually necessitating a heavy cast plate upon which the mechanical components are mounted. For the Small Boy environment, an even more rigid assembly was required, which in this case took the form of a box-shaped aluminum casting.

This transport, originally designed for use in rocket sleds for the U. S. Air Force, was capable of properly operating during 50-g accelerations. It included an armored take-up-reel housing to protect the tape record even in the event of severe tape transport damage. This machine, which was designed to handle a sufficient quantity of 1-inch wide, 1.5-mil thick tape for a total recording time of 45 seconds at a linear tape speed of 120 in/sec, was successfully used in the Diamond Ordnance Fuze Laboratories (DOFL) Operation Plumbbob recorder.

A redesigned version of the (MR 31E Cook) transport proved suitable for use in the recorder.

The basic machine, which provided ample mechanical characteristics with respect to shock and vibration, was modified to accept two 7-channel recorders.

The increased friction resulting from moving 1-inch tape at 120 in/sec over twice the head surface area required additional motor torque.

The transport was modified to accommodate a larger drive motor which was selected to provide speed regulation characteristics superior to the original unit. Tests on the redesigned tape transport disclosed that the flutter and wow was reduced to 0.3 percent peak-to-peak from the original 1.0 percent.

The larger drive motor, which was a 24-volt dc vibrating-reed-speed-regulating type unit, was capable of accelerating from rest to full constant speed, with a tape load in about 5 seconds.

A DOFL-designed precision clock-motor-driven timing assembly was included as part of the transport and was connected to the sequence timer. This timing assembly was activated by the −1 minute relay closure and effected the sequence of steps listed in Table 2.3.

Scotch 991 tape, which is 1 mil thic , allowed an additional tape to be stored on the 4-inch transport reels. The smaller ratio of supply-reel tape diameter to take-up reel tape diameter changes during the actual recording time and contributes to improvement in speed, accuracy, and flutter reduction.

2.5.4 Integrators. Since the input to the system was the output of a loop antenna and hence very nearly proportional to $\frac{dH}{dt}$, integrators were included in each channel to convert the signals to H. The integrators performed their function properly over a relatively small dynamic range due to limitations imposed by rate-gain, signal-to-noise ratio, and long and short term drift and noise problems inherent in transistorized, wide-band, high-gain dc amplifiers. Therefore,

at least three recording channels were assigned to each input sensor. Each group of three channels was designed to bracket the expected signal input from a specific sensor. In general, the inputs were arranged to provide a channel designed to handle the expected signal level, a channel one order of magnitude above, and a channel one order of magnitude below the level. In some instances, different integrators provided the required signal sensitivity by rate gain adjustment, and in other cases, depending upon the station location, input attenuators were added. To simplify the manufacturing and service problems, the integrators were divided into six groups that provided units which could perform all of the required functions satisfactorily.

The integrators provided at their output a signal which was the time integral of the pulses applied to their inputs. Each integrator consisted of a high-gain amplifier, a computing network (input and feedback components), and an output coupling network. Two general types of integrators were provided: one employed a commercial operational amplifier, the other used an operational amplifier designed by Rixon especially for this application.

The integrator provided an output which, in general, is

$$E_0(t) = \int G_R \, E_i \, (t) \, dt,$$

where $E_0(t)$ = output, volts

$E_i(t)$ = input, volts

G_R = rate gain, sec^{-1}

For a rectangular input pulse of width T and peak amplitude E_i, the output of the integrator is a ramp signal which terminates at the end of the input pulse, with a peak (final value at that time) given by (see Figure 2.8)

$$E_0 = G_R E_i T$$

and

$$G_R = 1/RC$$

where E_0 = peak value of output signal, volts

G_R = rate gain, sec^{-1}

R = input resistor, ohms

C = feedback capacitor, farads

E_i = input pulse amplitude, volts

T = input pulse duration, seconds

The nominal full-scale output voltage is ± 10 millivolts. However, integrator performance remains linear, without overload, to levels of at least ten times that value, at which value other elements in the system are fully saturated. Rate gains from 10 to 250,000 were provided.

Differential signal inputs were provided through identical circuits for each input. These were adjusted to precisely the same RC product, to provide good common-mode rejection;

that is, rejection of the inphase components of signals on the two inputs.

When the input signal returns to zero, the integral remains constant at the (non-zero) value given above. However, in practice, the integrator output E_0 slowly decays to zero, following the function

$$E_0 = E_0 \; e^{-t/ARC}$$

This simple exponential decay has a time constant, T_a, given by

$$T_a = ARC,$$

where R and C are as before, and A is the amplifier gain, usually the open-loop gain, in this case well in excess of 10,000. But, in this case, the gain was restricted, by means of feedback, to minimize difficulties from drift (which is proportional to gain) so that

$$A = R_f/R,$$

and consequently

$$T_a = R_f C$$

provided only that G, the open-loop gain meets the criterion $G \gg A$. The integrator output contained, in addition to the integral, various noise signals, and in fact, the integrator noise characteristics of necessity were a principal factor in establishing the system dynamic range. Peak-to-peak

short-term noise and drift approximated 5 percent of nominal integrator full-scale output, while long-term noise and drift seldom exceeded 20 percent.

Finally, the amplifier was ac-coupled to its output load to discard the lowest frequency components of drift, using an RC high-pass filter having a coupling time constant, T_c, given by:

$$T_c = R_L C_c$$

where R_L is the input impedance of the load on the integrator (VCO) and C_c is the coupling capacitor.

The overall decay time constant of the entire integrator circuit, T_d, varied from 1 millisecond to 4 seconds, depending on rate gain, with values of T_c as great as 10 seconds. For such large values of T_c, driving the 40,000-ohms imposed by the VCO which followed, values of C_c of the order of 1,000 microfarads were required, necessitating the use of tantalum electrolytic capacitors in parallel.

The standardized nominal values of integrator rate gain and their related decay time constants are specified in Table 2.4.

For the highest two rate gains, only a short decay time constant was required, for which a low amplifier gain was adequate, with resulting reduced noise and drift. For these

two rate gains a commercial operational amplifier (Philbrick) was used in lieu of the Rixon-designed operational amplifier, resulting in the P-65 integrator shown schematically in Figure 2.9. The other rate gains use the Rixon integrator of Figure 2.10.

2.5.5 Voltage Controlled Oscillator. General. The recording system included a data-channel bandwidth extending from dc to approximately 300 kc, i.e ; it could resolve an input pulse with a rise time of 1.5 μsec. This continuous data bandwidth was achieved by the ± 30-percent modulation of a 710-kc carrier.

This resulted in an FM signal with a modulation index $M_f = \frac{\Delta f}{f_m} = \frac{213}{300} = 0.71$. With such a numerically low modulation index, the major portion of the intelligence was contained in the carrier and first two side band pairs.

The VCO was a transistorized multivibrator type device provided with a modulation circuit capable of accepting signals and producing FM output to meet the above characteristics.

Design. The Vector Model TL-61-BDF VCO was designed to meet the following specifications:

1. Input Sensitivity: ± 10 mv or 0 to 20 mv (offset control provided to adjust input continuously between these limits.)

2. Modulation Characteristics. 710 kc ± 30 percent. (Control provided to adjust modulation percentage up to 40 percent.)

3. Input Characteristics. Differential input, dc to 300 kc, ± 1 db.

4. Common Mode Rejection. dc - 120 db min, 300 kc - 30 db min.

5. Z_{in} equals 40 K in parallel with no more than 100 pf.

6. Z_{out} equals 1 K with floating output (i.e., ungrounded).

7. Output at least 8v across 3 K.

8. Linearity. Within plus or minus 1 percent from best straight line.

9. AM output. Less than ± 1 db.

10. Power. 25v at 120 ma.

11. Stability. Power change of plus or minus 10 percent in the 25v supply will change center frequency less than ± 3 percent of design bandwidth.

12. Drift. After 15 minute warm-up, total center frequency (cf) drift shall not exceed ± 10 percent of absolute frequency in any 8-hour period nor exceed ± 0.5 percent of absolute frequency in any 10-minute period.

13. Temperature Compensation. From 10° to 50° C. Over this temperature range, cf shall not change more

than ± 5 percent absolute frequency and bandwidth shall not change more than ± 2 percent of its design value.

14. Units were potted in Isofoam for shock resistance in a metal cubical box with dimensions not exceeding 1.5 by 1.5 by 2.5 inches.

A standard VCO requires an input signal of ± 2.5 volts to fully modulate its carrier. The Model TL-61 BDF was required to be fully modulated with a ± 10 millivolt signal and therefore was designed to include a differential dc amplifier to increase its input sensitivity to this value. In order to maintain the differential characteristics in the basic VCO design, it was necessary to include a dc-dc converter in the VCO module which isolated the dc-amplifier circuitry from the main battery supply.

The overload characteristics of the VCO were such that it would accept a maximum positive going signal of 17 mv, (i.e., driving the oscillator higher in frequency) and a maximum negative going signal of approximately 25 mv (driving the oscillator lower in frequency). The VCO was therefore polarity oriented in the system so that the negative going field signal would frequency-modulate the VCO downward in frequency. Since the predicted input signal exhibited a negative peak swing, which was greater than a positive swing, an effective appreciable increase in system dynamic range resulted.

2.5.6 Record Amplifier. The record amplifier was designed to provide a constant current drive to a magnetic head. One record amplifier was required for each track.

The amplifier, which consisted of a transistorized differential input-differential output unit, was packaged as a plug-in printed circuit card. It was designed to provide a constant current head drive signal over a frequency range extending from 100 kc to 2.5 Mc so that it could be used either for high frequency bias or non-bias recording. The amplifier was designed to accept two inputs: first, the bias signal of 1.85 volts RMS at 2.5 Mc at an impedance (presented by the amplifier input) of 3,000 ohms; second, a differential signal input intended to be driven from the 710-kc VCO deviated a maximum (nominal ± 30 percent) of + 65 percent/−80 percent, which would yield components from 100 kc to 1.25 Mc.

The amplifiers required that in non-bias recording, the input signal source (VCO) have an output impedance no greater than 1,000 ohms and supply 1.85 volts RMS to a load of 3,000 ohms, which was the impedance presented to each VCO output by the amplifier. The amplifier had the following characteristics:

1. Output (max): 2.5 Mc, 13 ma into each half of the split head winding; from 100 kc to 1.25 Mc, 1.3 ma into

each half of the split head winding.

2. Distortion: Over frequency band and level conditions in (1) above, less than 1 percent.

3. Phase Response: Constant from 100 kc to 1.25 Mc such that the shape of the FM input signal envelope is not distorted.

4. Common Mode Rejection: No less than 20 db (at differential output).

The schematic of the record amplifier is shown in Figure 2.11.

The input, which consisted of a constant voltage signal varying in frequency from 100 kc to 1.05 Mc, was applied to the base of Q301 and formed a differential amplifier stage. The outputs of Q301 and Q302 were applied to a second differential amplifier stage, Q303 and Q304. The outputs of the second amplifier stage were applied through emitter followers to the output transistors, Q308 and Q309. The emitter followers served as buffers between the differential amplifier and the high current output stage.

A feedback voltage was taken from the collector of Q303 and applied through R318 to the base of Q302. The voltage gain of the differential amplifier was determined by the ratio of R318 to the signal input resistor R304. Since this feedback circuit affected the collector load of Q303, a similar load,

R317 and C307, was connected to the collector of Q304 to ensure that the differential amplifier remained balanced.

The output stage, consisting of transistors Q308 and Q309, was essentially a pair of common-emitter amplifiers with unbypassed emitter resistors which functioned as constant-voltage to constant-current converters. The base drive to this circuit was a constant-voltage signal which, due to the low base-emitter impedance, also appeared at the emitter. The constant-voltage signal at the emitter provided a constant emitter current, related to the signal voltage by the 243-ohm emitter resistor. This constant current by transistor action also flowed in the collector circuit. Thus, the recording head current was constant for a constant-voltage signal regardless of the variation of head impedance with varying frequency. Inductors L301 and L302 provided a dc return for Q307 and Q308 but appeared as an open circuit to the signal frequencies.

The dc voltages at the differential amplifier outputs were balanced by potentiometer R307. Transistor Q305 operated as a constant-current source, providing the large dynamic emitter impedance for Q303 and Q305 which was required for balance differential operation. Resistor R316 and capacitors C305, C306, and C307 were stabilizing networks which prevented oscillations from occurring within the amplifier.

Complete stability of each recording channel was further insured by a ground from the center tap of the record-head coils. Although the head coils were well balanced, the current required for good recording was near that which produces magnetic saturation, and the resulting nonlinear magnetic performance could permit a switching transient or heavy overload to cause the channel to oscillate. A head-coil center tap ground minimized the unbalanced components of head current and reduced the coupling between the two halves of the head, preventing magnetic nonlinearity at the operating level.

2.5.7. Fiducial Markers. A fiducial and a timing signal were used to accurately establish time zero on each head stack and to provide continuous time calibration, both as aids in data analysis.

An externally generated fiducial marker signal was shaped and mixed with a highly stable internal crystal oscillator and fed to a single VCO input. The VCO output was fed to parallel-connected Channel 7 and Channel 8 record amplifier inputs. A single VCO was used to preclude the random phase relation between two free running VCO oscillators resulting in a phase displacement and/or jitter between timing signals on one head stack with respect to the other.

Two types of fiducial markers were used. In all pits and bunkers where short cable runs could be made gamma-ray-sensitive fluors were used. At the 100-foot-deep station where long cable lengths obviated the use of a gamma ray detector, due to possible electromagnetic (EM) pickup, a Teller light detector was used.

Gamma Fiducial Marker. The system consisted of plastic fluor, fluor light attenuator, photodetector, voltage supply and output signal networks, and a suitable mechanical mounting system.

The detector assemblies were mounted in 4-inch diameter aluminum tubes with a 0.250-inch wall thickness. A weldment flange was on this tube so that the tube protruded 6 inches above the ground surface. The other end extended down into a steel casing which was 6 inches outside diameter with a 0.125-inch wall thickness. This steel tube extended down 30 inches into an 8-inch-diameter hole in the concrete base.

A cup which held the fluor was placed at the top of the 4-inch-diameter aluminum tube. The photodiode or photomultiplier was mounted lower in the tube, the distance from the fluor being determined by the light attenuation system required by conditions at a given station.

The above mentioned detector mounting was covered with a 1-inch-thick aluminum dome.

The voltage requirements for the electronic circuit inputs were 5 to 10 volts at the pit recorders, (Stations 519.01 to 519.11), and 10 to 20 volts for the bunker stations (5-602 and 5-603); the above voltages were developed across a 50-ohm load. At Station 5-600 a 7-volt signal was developed across a 20-ohm load. This requirement called for currents of 100 to 200 ma from the pit detectors and 200 to 400 ma from the bunker detectors. Saturation-type detector circuits were used so that a constant output would be achieved over a wide operating range of input light fluxes. The voltage on the photodiodes was adjusted to give the desired current output under current saturation. The photomultiplier dynode potentials were developed across an empirically determined resistance string which gave the required current capability under saturation light inputs.

The plastic fluors in the form of discs (2-1/2-inch diameter by 2-inch thickness) were cut and polished from NE 102 plastic fluor stock. These were placed in the fluor cups with the exit aperture in the cover plate.

Light from gamma ray conversion in the fluor was, in some cases, attenuated to give the desired light input to

the detectors. To accomplish this, the distance was varied between the fluor and the detector. This system was also instrumental in placing the photomultiplier below ground to minimize the effects of electromagnetic pickup. To achieve further light attenuation, when required, apertures were placed at the fluor and the detector. Fluor-to-detector distances and the aperture diameters are shown in Table 2.5.

Power for each photodetector and photomultiplier was supplied from its associated electronic recording unit or bunker. The recorders provided 1,000 volts at 2 ma. RG59/U cables and high voltage IPC fittings were used to connect the power supplies in the pit stations to their associated detectors, and RG 58/U cable with standard BNC fittings was used for signal leads at the pit stations.

The power and signal leads were switched on as follows: the detector power in the pit recorders was switched on at T-4 minutes. The signal output line was tied directly to the electronic unit and was not switched. At bunker stations (A, C, and D) the detector voltage was turned on at a tentative T-4 hours when the bunkers were closed. The output signal line was switched on at T-3 seconds.

Teller Light Fiducial System at Station 519.05. The fiducial trigger could not be obtained by the usual method of

exciting the photomultiplier with light from converted gammas in a fluor. The reason was that electrical leads to the surface could not be tolerated because of possible electromagnetic interference with the field measurements. The scintillator could have been put on the surface with a photomultiplier 100 feet below; however, we elected to use Teller light sent through a hole in the shaft plug to the detector at the bottom of the shaft to provide the trigger. A periscope was mounted above the hole in the plug so that the direct light could be utilized (Figure 2.12). Unfortunately, this fiducial marker did not work during the shot. Postshot examination did not yield any definite reasons for the failure.

Temperature Inside the Detector Mounting Tubes. Temperature recordings were taken inside the detector mounting tubes to determine the possibility of damage to fluors and photosensitive devices.

The 1,600-foot pit detector, Station 519.03, and the Bunker B detector station were selected. Both stations were in direct sunlight. The temperatures were measured with a Ryan Model D recording thermometer. This recorder was suspended inside the aluminum detector mounting tube with its center located 7 inches below the top of the tube.

Temperature measurements are recorded in Table 2.6.

2.5.8 Timing Oscillator. The timing oscillator was a modified Clapp circuit with a quartz crystal for frequency control. The crystal replaced the inductor normally used in this type oscillator, and since the frequency range in which the crystal appears inductive is very narrow, it established a high degree of frequency stability by sharply limiting the frequency range of the signal.

The oscillator stage, Q402 on the schematic, Figure 2.13, was a common-emitter amplifier. The signal at its collector was fed through the frequency-selective crystal feedback network, shifted in phase by 180 degrees, attenuated, and returned to the base. The feedback network consisted of Y401, a 100-kc quartz crystal in the timing application, C404, C403, R403, and C402. Capacitors C403 and C405, together with resistor R401, had values selected so that each shifted the signal phase by 90 degrees and attenuated it. Then with the gain and 180-degree phase shift of Q402, the conditions for oscillation were established in the feedback loop, namely gain greater than unity and zero phase shift at the frequency of oscillation. Capacitor C404 was variable to allow for compensation of slight differences in crystal frequencies and could pull the frequency about ± 25 cps. Inductor L401 provided

a dc return for Q402, and together with capacitor C405, formed a parallel-resonant circuit which increased the signal stability and aided in reliable starting by ringing on circuit noise until oscillations began to build up.

To insure stable operation with low distortion, the feedback current must be kept small to prevent overdriving the crystal. The feedback was returned to the base of the oscillator stage through Q401, an emitter-follower stage with a high input impedance and a low output impedance. Resistors R401 and R402 established a dc bias at a base of Q 401.

Stable operation requires that loading of the oscillator be minimized. The most harmful loading effects felt by an oscillator are those due to the output, particularly when the output load is variable. To eliminate these loading effects, cascaded emitter-followers were placed between the oscillator and the output. This cascading of Q403 and Q404 presented a high impedance to the oscillator, together with an output impedance of only about 10 ohms. The output of the oscillator proper was taken from the junction of the crystal, R403, and C403, a point of high amplitude and low distortion, and was fed through C410 and the output-amplitude potentiometer, R408, to the base of Q403. The final output signal was taken from the

emitter of Q404.

A stable oscillator supply voltage is a further requirement for frequency and amplitude stability. Two Zener diodes, CR401 and CR402, established this voltage. The 25-volt dc input voltage was dropped across R406, clamped at 11 volts by the Zener diodes, and bypassed by C408 and C409 to establish a very low supply impedance at higher frequencies. Two diodes were used so that each operated very near the voltage at which it displayed a temperature coefficient of zero.

2.5.9 Fiducial Mixer. The fiducial mixer consisted of a monostable multivibrator for fiducial signal reshaping, resistive mixing networks for mixing this signal with the 100-kc oscillator, and an adjustable dc voltage.

The dc voltage was used to set the associated VCO to a rest frequency of about 635 kc. The output level of the timing oscillator was then set to modulate the VCO to ± 15 percent, or half of normal, with deviation limits of about 520 and 750 kc. The monostable multivibrator, when triggered, then drove the VCO hard against its upper frequency limit of about 1.2 Mc, with sufficient overdrive to override the 100-kc signal, for a period of about 20 μsec.

The schematic diagram of the fiducial mixer plug-in card is given in Figure 2.14. The input pulse, which should

be a negative pulse of at least 1-volt amplitude and no more than 50 nsec rise time, was applied to an attenuator consisting of resistors R718 through R721, which may be used to adapt to much larger input pulses. The 1-volt sensitivity applies when R721 is removed and R718 and R719 are replaced with jumper wires.

The pulse was differentiated in capacitor C701 and resistor R701 and coupled (through diode CR701, which passed only the negative portions) to transistor Q701. This transistor, together with Q702, formed a conventional monostable, or one-shot multivibrator. Diode CR702 in the base of Q702 served to prevent application of excessive reverse V_{BE} to Q702 and also isolated thermal variations of I_{CBO} in Q702 from the timing network, C702 and R704, for improved thermal stability. Diode CR703 clamped the swing of the collector of Q702 to the voltage developed across Zener breakdown diode CR705, thereby greatly improving the rise time of the output pulse, which in turn was developed across R708 and R709 in series, where R708 provided a smaller, voltage-divided output.

The pulse from R708 was ac-coupled to the input of the VCO along with a dc voltage of about 2.5 volts, developed by voltage dividing in R710 and R711, the voltage developed across Zener breakdown diode CR704. The latter was chosen to be

about 5 volts, to approach a zero temperature coefficient.

The voltage across CR704 was also voltage divided at the arm of potentiometer R715 and applied through R716 to the other (+) input of the VCO, permitting the dc-voltage differential between the VCO input terminals to be set to either polarity and from zero to tens of millivolts for rest-frequency adjustment. The 100-kc timing signal was ac-coupled to the + input, after voltage division in resistors R713 and R714.

2.5.10 Patch Cards. Patch cards were used to facilitate simple trouble-free, prearranged, and rapid interconnection of the input sensors to data channels (integrators) in any chosen combination.

Each input connector was carried to both patch cards, while half (six) channel inputs appeared on each card. All of these leads were carried to solder lugs, so that short-soldered jumper wires on the proper card would connect any sensor to any channel.

Each input sensor was terminated in a single terminating and attenuating circuit, which could be common to several channels. Two such terminations were provided on each patch card, so that between them both, four differential sensors were terminated.

The schematic of the patch card is shown in Figure 2.15. The differential signal was applied across resistors R802, R803, and R804 (or R816, R817, and R818 for the other channel). The arm of R803 was connected to the ground return and adjusted for exact balance, to minimize the common-mode signal. Resistors R805 through R809 performed a similar function, except that they provided balanced voltage-divided outputs at a five-to-one attenuation. Resistors R810 through R814 constituted the fifty-to-one balanced attenuator. Resistor R801 padded the input impedance down to precisely 300 ohms.

Resistor R829 and capacitor C801 terminated an unbalanced gamma or spare channel. The 75-ohm R829, in parallel with attenuators placed in the integrator compartments, terminated the line in approximately 50 ohms, while this impedance and C801 formed an RC integrator of about 1-microsecond time constant.

Resistors R829 and R830, together with diode CR801 and double-anode Zener breakdown diode CR802, constituted the special power-supply network for integrator coupling-capacitor forming, placed on the patch cards because it was common to all the integrators.

2.5.11 Automatic Sequencing System. The recorder package was designed to be completely self-contained and

automatic. It contained an automatic sequencing system which was responsive to Edgerton, Germeshausen and Grier (EG&G) timing signals (relay closures) until slightly prior to time zero, whereupon it disconnected itself from external control and switched to an internally programmed event sequence specifically tailored to the system's needs. It was not only no longer subject to external control, but it also disconnected internal circuits from the external control lines to preclude their acting as antennas which might pick up very large signals and introduce them inside of the multilayer magnetic shields to circuits. Sufficient sophistication was built into the timing system so that in the event of a hold prior to time zero minus 5 minutes it would reset itself. At minus 5 minutes the system was committed, since it could no longer recycle. After minus 55 seconds, the timing lines were internally disconnected.

The internal sequencing system, following a carefully planned sequence, connected power to the various elements in the system to allow adequate warm-up of the electronics; to charge, electroform, and discharge the large tantalum electrolytic capacitors in the integrator circuits; and to allow sufficient time for the tape transport drive motor to accelerate to full speed, all with minimum drain on the battery supplies.

A large degree of reliability was designed into the sequencing system to preclude a malfunction occurring. For example, the external EG&G timing signals closed relays which placed circuits in operation and also started an internal clock timer which after a suitable delay locked in the externally triggered relays so that the circuits that they controlled could no longer be influenced by subsequent signals on the timing lines. Moreover, the more important relay contacts were paralleled by rotary step switch contacts that were not subject to opening momentarily under high-g forces which may be present slightly after the event.

The complete time-versus-operation sequence is shown in Table 2.3.

2.6 PLAYBACK SYSTEM

The playback system consisted of a multichannel wide-band instrumentation tape recorder and discriminators. A fourteen-channel Mincom CM-100 was used. This machine had a flat (within 3 db) frequency response from 400 cps to 1.2 Mc at 120 in/sec tape speed. This bandwidth was sufficient to recover all significant side bands of the FM system. Playback was generally done at 12 in/sec, one tenth record speed, to reduce head and tape wear. The carrier frequency then became 71 kc.

The discriminators used were Ampex FR 600 modified for a center frequency of 71 kc. Twenty and forty kc, linear-phase, output filters were used interchangeably. These corresponded to 0- to 200-kc and 0- to 400-kc information bandwidths in real time. The former was used for data channels and the latter for timing and fiducial

marker channels.

A Tektronix 555 oscilloscope was generally used for readout. The oscilloscope was generally triggered from the fiducial marker; however, in some cases gap scatter and azimuthal misalignment of the heads necessitated internal triggering.

2.7 SYSTEM CALIBRATION

Each recording channel was calibrated both before and after the shot by two methods and an average calibration constant determined.

In the first method, a signal was impressed at the input of the recording channel by means of a special calibrating circuit. The output of this circuit was a pulse whose shape and amplitude were accurately known. The resultant channel output was recorded on tape and a calibration constant, of the playback, in terms of volts of discriminator output per volt-second of input, was determined. This constant, when multiplied by the antenna constant, as determined by the method described in Section 2.4, yielded a final calibration of discriminator output per unit magnetic field. A magnetic tape for each recorder was run before and after the shot.

The second method consisted of placing the antenna in the known magnetic field (a damped sine wave of measurable amplitude) in a Helmholtz coil. The current in the coil, which is proportional to the generated pulse, was monitored on one channel of a dual-beam scope. The output of the antenna was then fed, through a cable of the same type and length as used in the shot, into the proper

recording channels. The resulting frequency-modulated current in the recording head was monitored and fed into the discriminator. Since the discriminator output is independent of input amplitude beyond a given threshold, it is immaterial whether it receives its signal from the playback of a tape or directly from the recording head as in this method. The output of the discriminator was displayed on the second channel of the dual beam scope, with the Helmholtz coil current on the first. The ratio of the two recorded voltages, multiplied by proper constants, yielded the desired discriminator output per unit magnetic field. The numbers thus obtained were in close agreement with those obtained by the previous method, and an average of the two was used.

TABLE 2.2 PROJECT 6.2 STATION LOCATIONS

Station Number	Ground Range	Direction
519.01	250	N43°E
519.02	625	N43°E
519.03	1600	N43°E
519.04	1650	N43°E
519.05	1600 (100 feet deep)	N43°E
519.06	4000	N43°E
519.07	9800	N43°E
519.08	1600	S58°W
519.09	625	N17°W
519.10	1600	N17°W
519.11	4000	N17°W

TABLE 2.3 ELECTRONIC RECORDER ASSEMBLY OPERATION SEQUENCE

ELECTRONIC RECORDER ASSEMBLY

OPERATION SEQUENCE

E.G.G. TIMING	INTERNAL TIMING	SEQUENCE SWITCH S5 POSITION	OPERATION	RESULT
-30 Mins.		1	Relay K3 activated.	+25 Volts to VCO
			Relay K4 activated.	-25 Volts and +25 Volts to Integrators Time Delay Relay K5 activated (-15 V. forming voltage (to Integrator Capacitors.
	-25 Min.		Time Delay Relay K5 transfers contacts	-15 Volts forming voltage removed from Integrator Capacitors and Capacitor circuit grounded.
	-20 Min.		Time Delay Relay K6 transfers contacts.	Time Delay Relay K6 activated. Integrator capacitor circuit opens.
-5 Min.			Timing Motor M1 starts.	
	-4 1/2 Min.	2	Sequence Switch S5 actuated.	Locks in +15 Volts to Integrator circuit. Locks in -15 Volts to Integrator circuit. Relay K1 (Connects two +25 Volt circuits (to Amplifiers. Relay K2 actuated (Locks-in +25 Volts to VCO. (Connects +25 Volts to DC-DC Converter. (Disconnects Integrator Capacitor circuit from Time Delay Relay K6.
	-3 1/2 Min.	3	Sequence Switch S5 actuated.	
	-2 1/2 Min.	4	Sequence Switch S5 actuated.	
	-1 1/2 Min.	5	Sequence Switch S5 actuated.	
-1 Min.			Timing Motor M2 starts.	Timing and Tape Pressure Plate Cams activated.
	-55 Sec.		Cam Operation	Switch S8 closes. Locks in Timing Motor M2.
	-30 Sec.	6	Sequence Switch S5 actuated	
	-20 Sec.		Cam Operation	Switch S9 closes (Transport Drive Motor M3 starts. (Solenoid Switch S10 actuated. 1. E.G.G. Timing Lines disconnected. 2. Relays K3 and K4 deactivated. 3. Time Delay Relays K5 and K6 deactivated and reset.
	+20 Sec		Cam Operation.	Switch S9 opens. (Transport Drive Motor M3 stops.
	+30 Sec.	7	Sequence Switch S5 actuated.	
	+40		Cam operation	Switch S8 opens. (Timing Motor M2 stops.
	+1 1/2 Min.	8	Sequence Switch S5 actuated.	Relay K1 actuated. (Disconnects two 25 v. circuits to amplifiers.
	+2 1/2 Min.	9	Sequence Switch S5 actuated.	+15 Volts disconnected from Integrators. +15 Volts disconnected from Integrators. Relay K2 actuated. (+25 v. disconnected from VCO & DC-DC Converter. (Integrator capacitor forming circuits reconnected, to Time Delay Relay K5 through K6.
	+3 1/2 Min.	10	Sequence Switch S5 actuated.	Timing Motor M1 stops.
		11 & 12	Reset positions.	

Note. Electronic reference designations apply to schematic Drawing No. E10974052TL.

TABLE 2.4 INTEGRATOR RATE GAIN AND DECAY TIMES

Rixon Model Number 905-	Nominal G_R v/vs	Nominal T_d seconds	Notes
3364 (07)	10	4	1
3364 (07)	100	4	2
3364 (07)	500	4	
3365 (08)	1000	2	
3366 (09)	5000	0.2	
3367 (10)	5000	0.1	
3360 (05)	50,000	0.005	
3361 (06)	250,000	0.001	

Notes:

1. Use integrator of G_R = 500 preceded by balanced-H resistive attenuator of 50/1 (located on plug in patch card).

2. Use integrator of G_R = 500 preceded by balanced-H resistive attenuator of 5/1 (located on plug in patch card).

TABLE 2.5 FLUOR TO DETECTOR DISTANCES AND APERTURE SIZES

Station Number	Station Distance (ft)	Detector Type	Scintillator to Detector Distances (inches) *	Aperture Diameter (inches)
519.01	250	Photodiode	6.0	No Aperture
519.02	625	"	1.38	"
519.09	625	"	1.38	"
5-600	625	"	1.38	"
519.03	1600	Photo-multiplier	22	0.250
519.04	1650	"	22	0.250
519.05	1600	"	22	0.250
519.08	1600	"	No fluor	No Aperture
519.10	1600	"	22	0.250
519.06	4000	"	12	0.500
519.11	4000	"	12	0.500
5-602	4000	"	12	0.500
519.07	9800	"	1.13	No Aperture
5-603	9800	"	1.13	"

* Indicates distance between photocathode and fluor.

TABLE 2.6 DETECTOR-MOUNTING-TUBE TEMPERATURE MEASUREMENTS

Date	Min. Temp. F°	Max. Temp. F°	Official NTS Temp. F°	Station
28 June	-	100	105	519.03
29 June	*77	*96	102	519.03
30 June	*70	*96	102	519.03
1 July	75	91	102	5-601
2 July	73	91	102	5-601

* A dome painted white was used while these data were taken. Natural cast aluminum domes were used during the other readings.

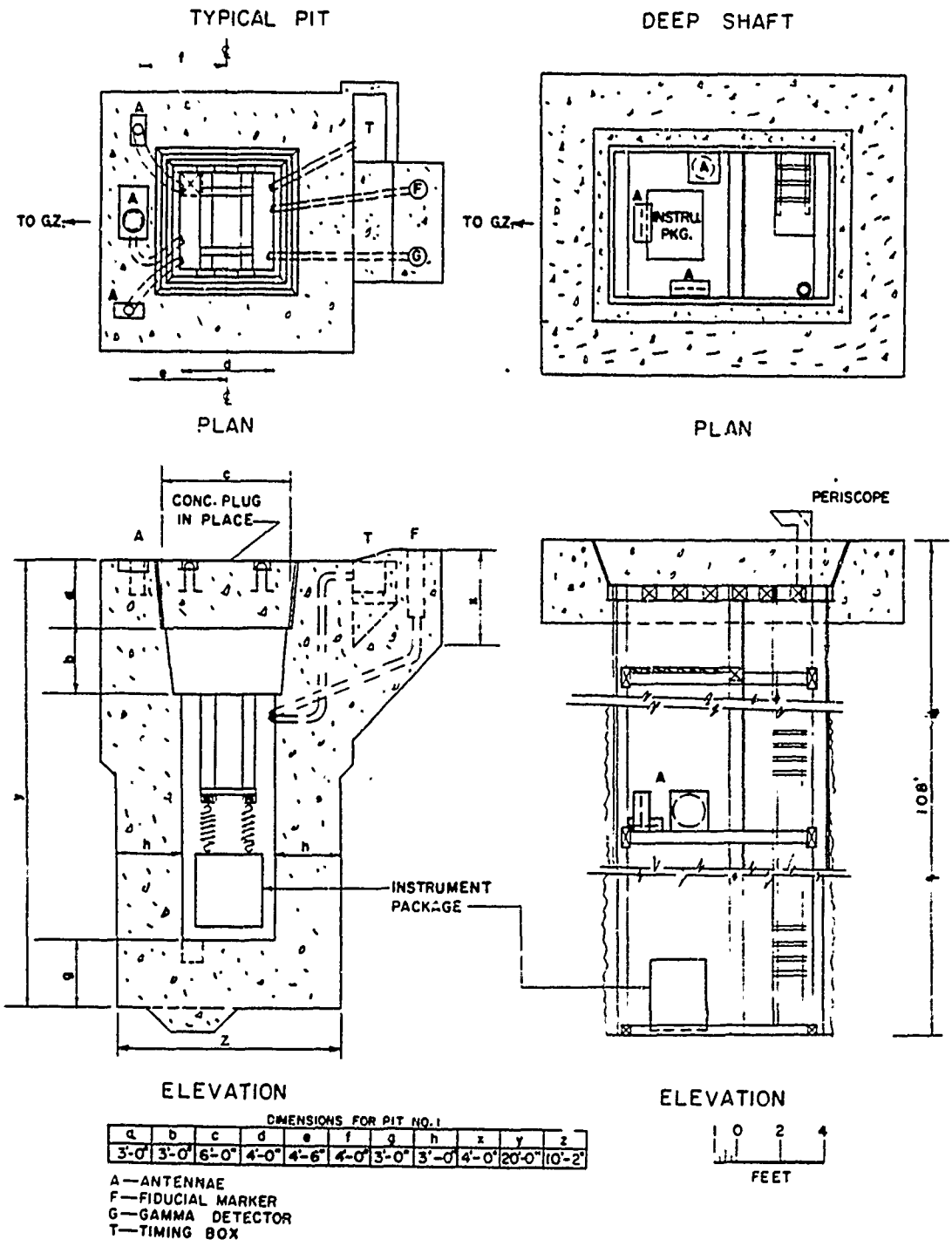

DIMENSIONS FOR PIT NO. 1

a	b	c	d	e	f	g	h	x	y	z
3'-0"	3'-0"	6'-0"	4'-0"	4'-6"	4'-0"	3'-0"	3'-0"	4'-0"	20'-0"	10'-2"

Figure 2.1 Project 6.2 pit station diagram.

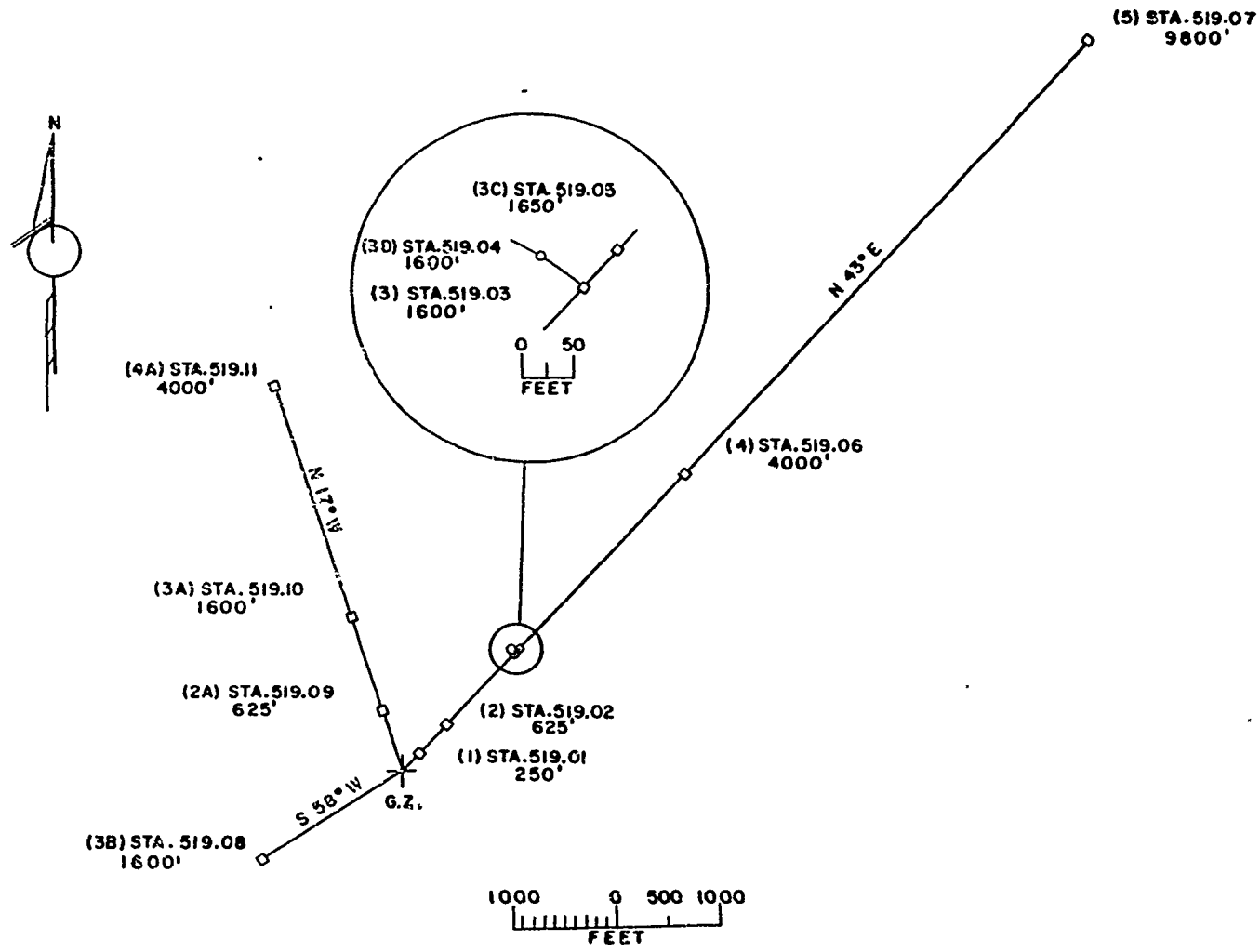

Figure 2.2 Project 6.2 station locations.

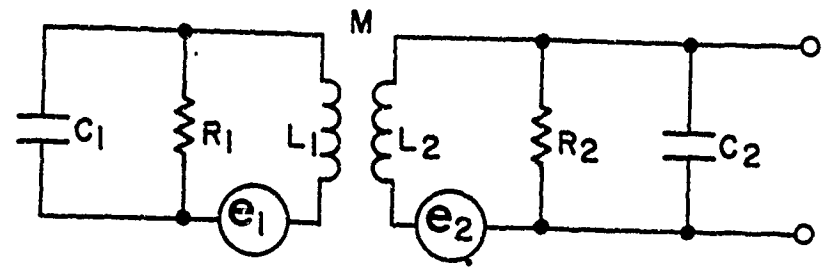

(a) Shielded Loop

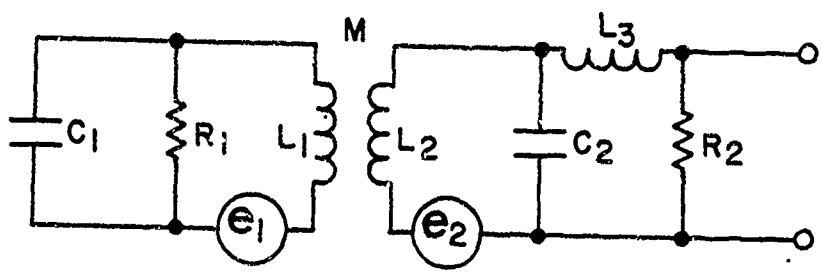

(b) Shielded Loop with Cable

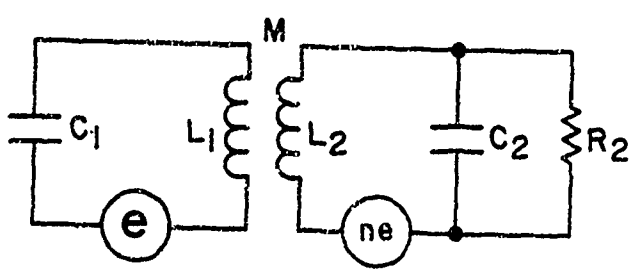

(c) Simplified Equivalent Circuit

Figure 2.3 Equivalent circuits for a shielded loop antenna.

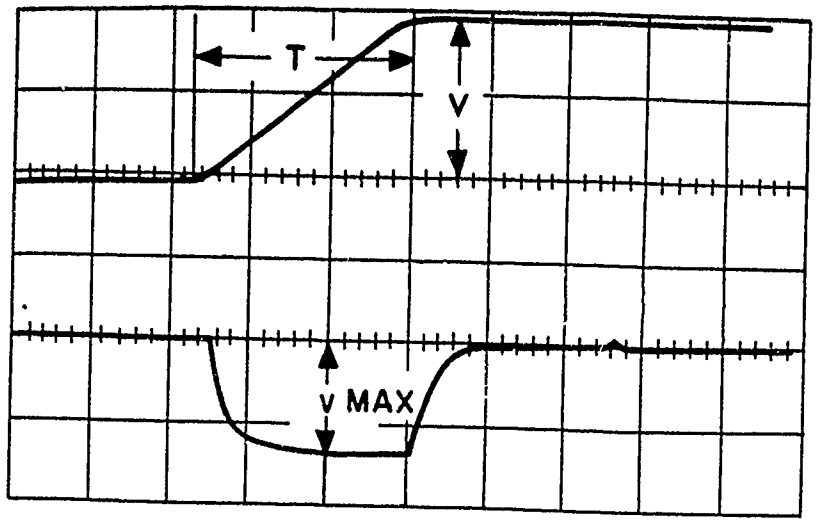

Upper trace - Voltage across series resistor

Vertical sens.	2 volts/cm
Horiz. sens.	20 microseconds/cm
v = 3.95 volts	T = 49.7 microseconds

Lower trace - Antenna Output

Vertical sens.	.010 volts/cm
Horiz. sens.	20 microseconds/cm

v_{max} = 13.5 millivolts

$k = 3.26 \times 10^{-7}$ volts/ampere turns/meter/sec.

Figure 2.4 Calibration of antenna.

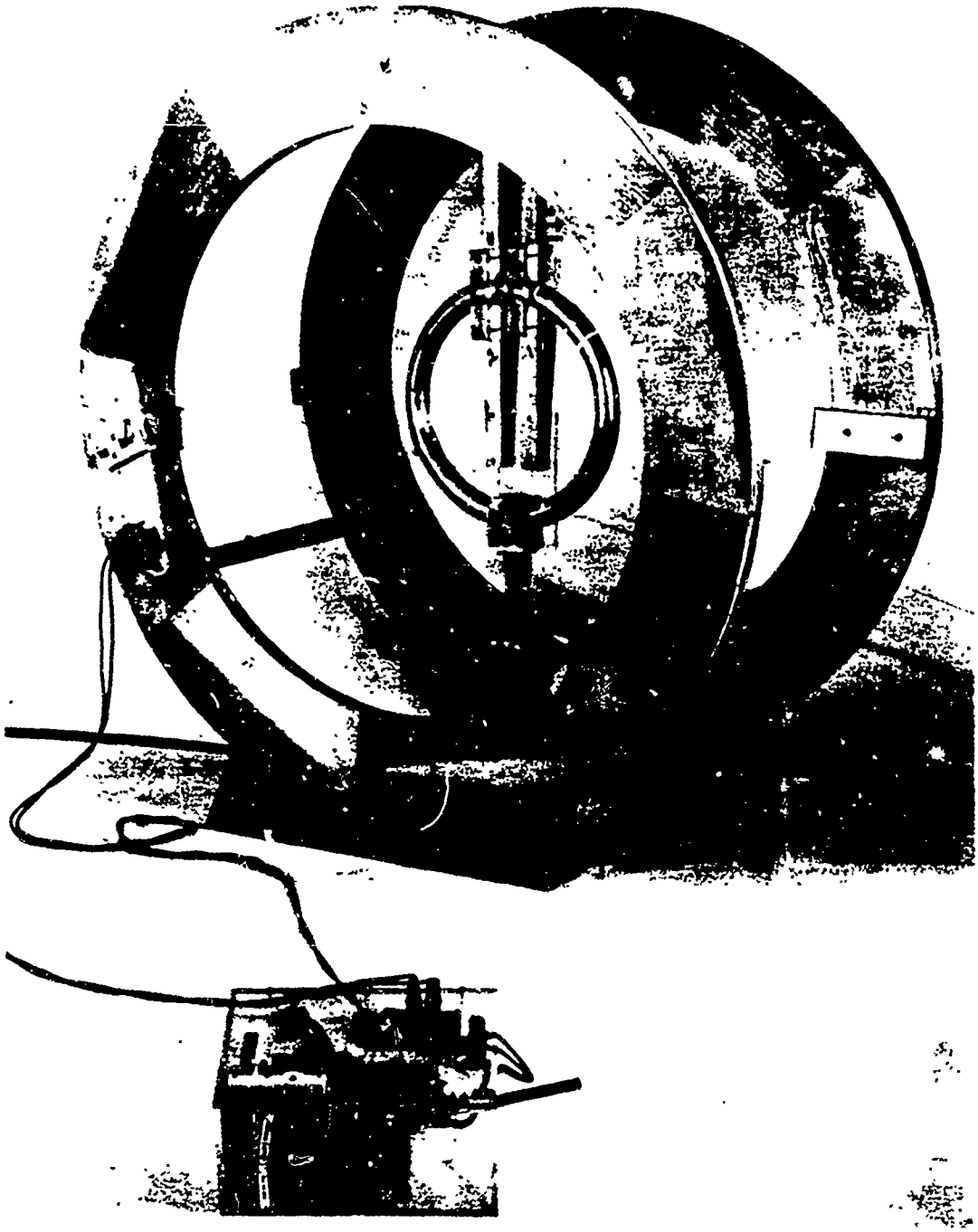

Figure 2.5 Experimental arrangement for calibration of antennas. (HDL photo)

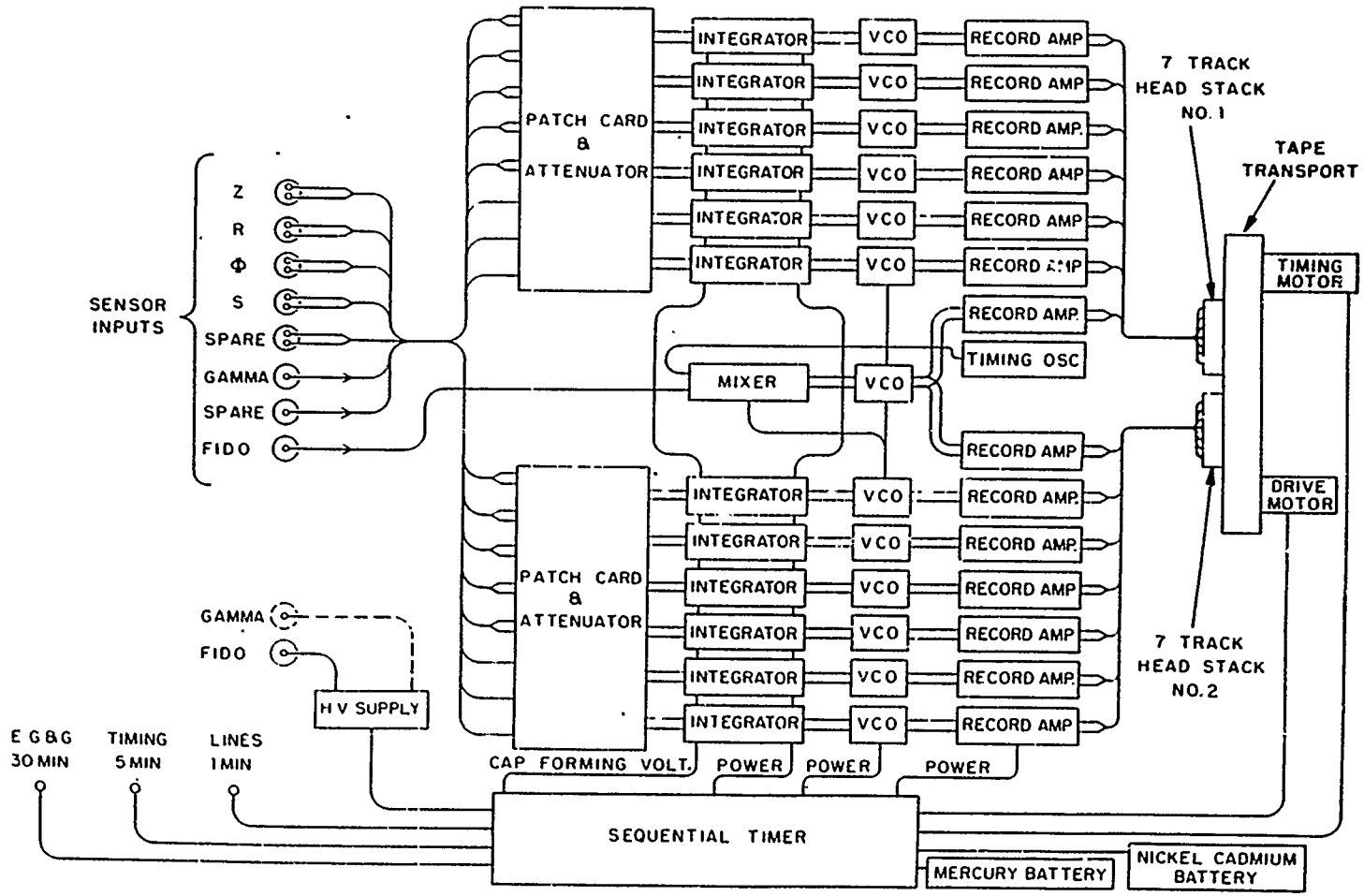

Figure 2.6 Block diagram HDL SB 1 recorder.

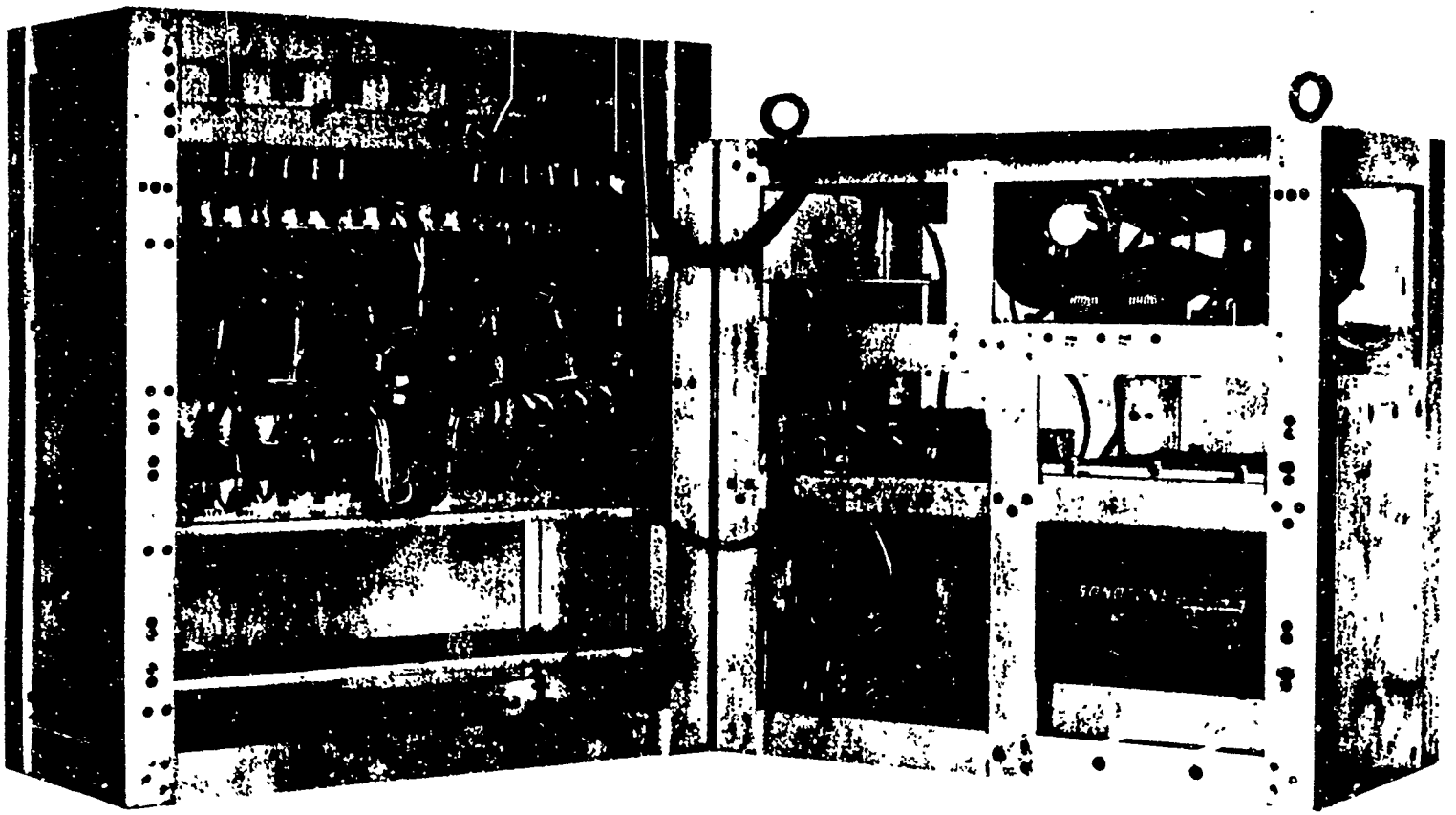

Figure 2.7 Small Boy recorder open for servicing. (HDL photo)

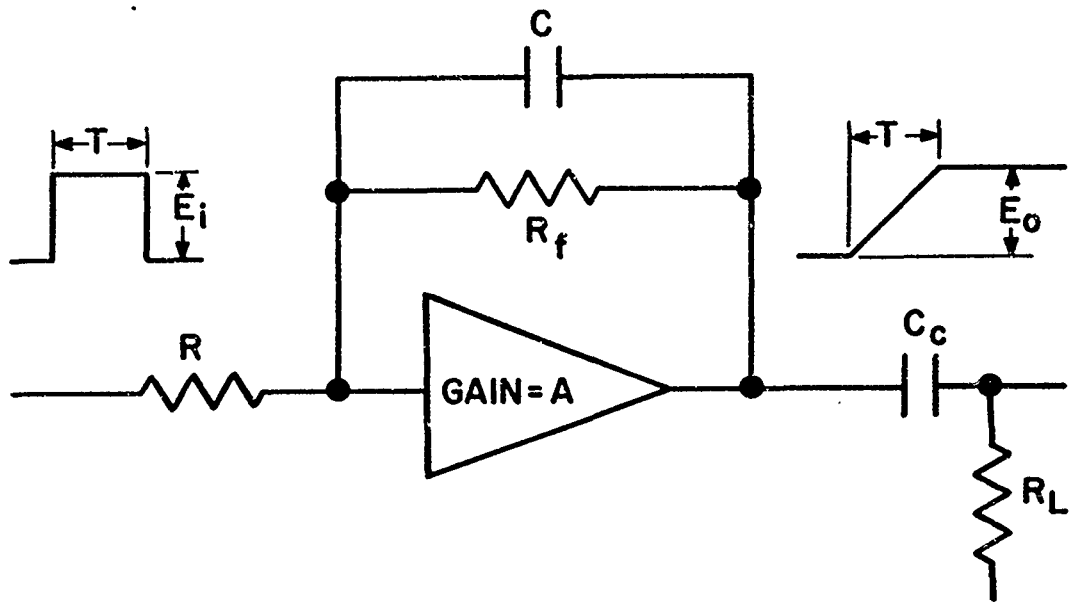

Figure 2.8 Conceptual diagram of integrator.

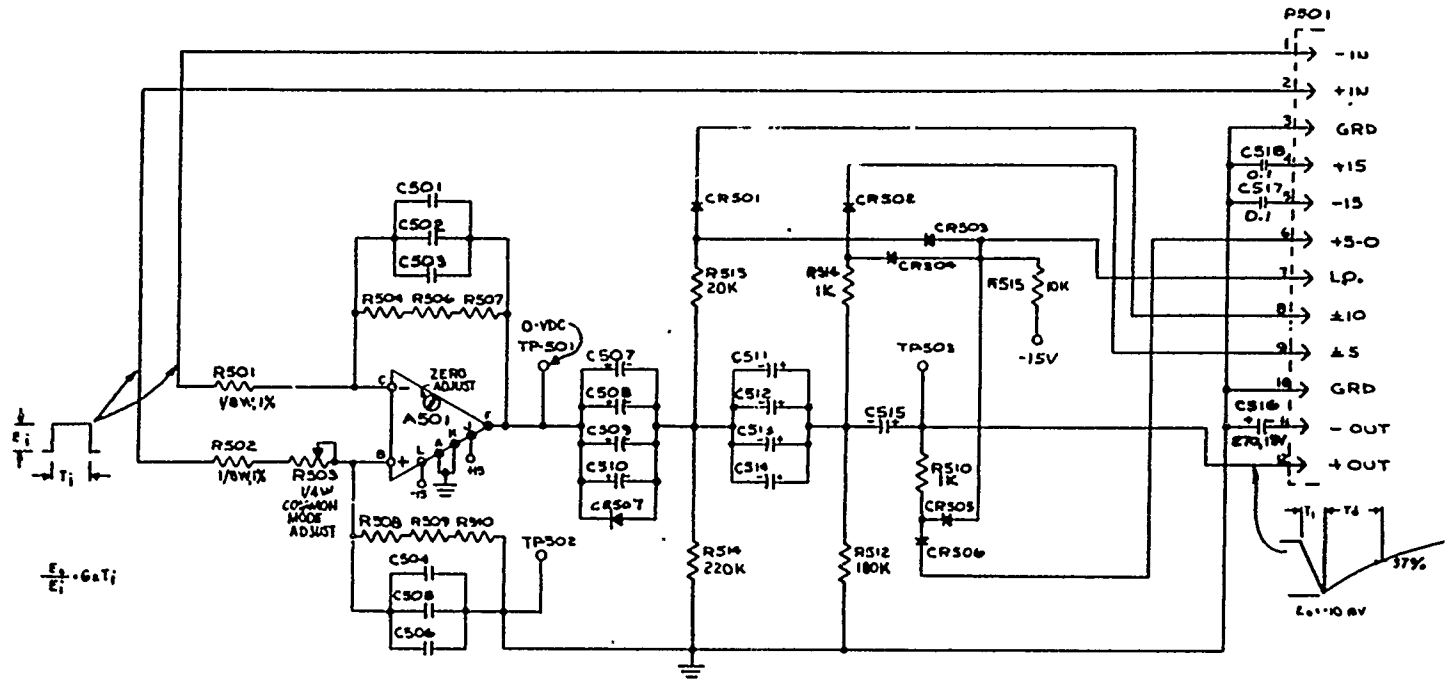

Figure 2.9 P65 integrator schematic.

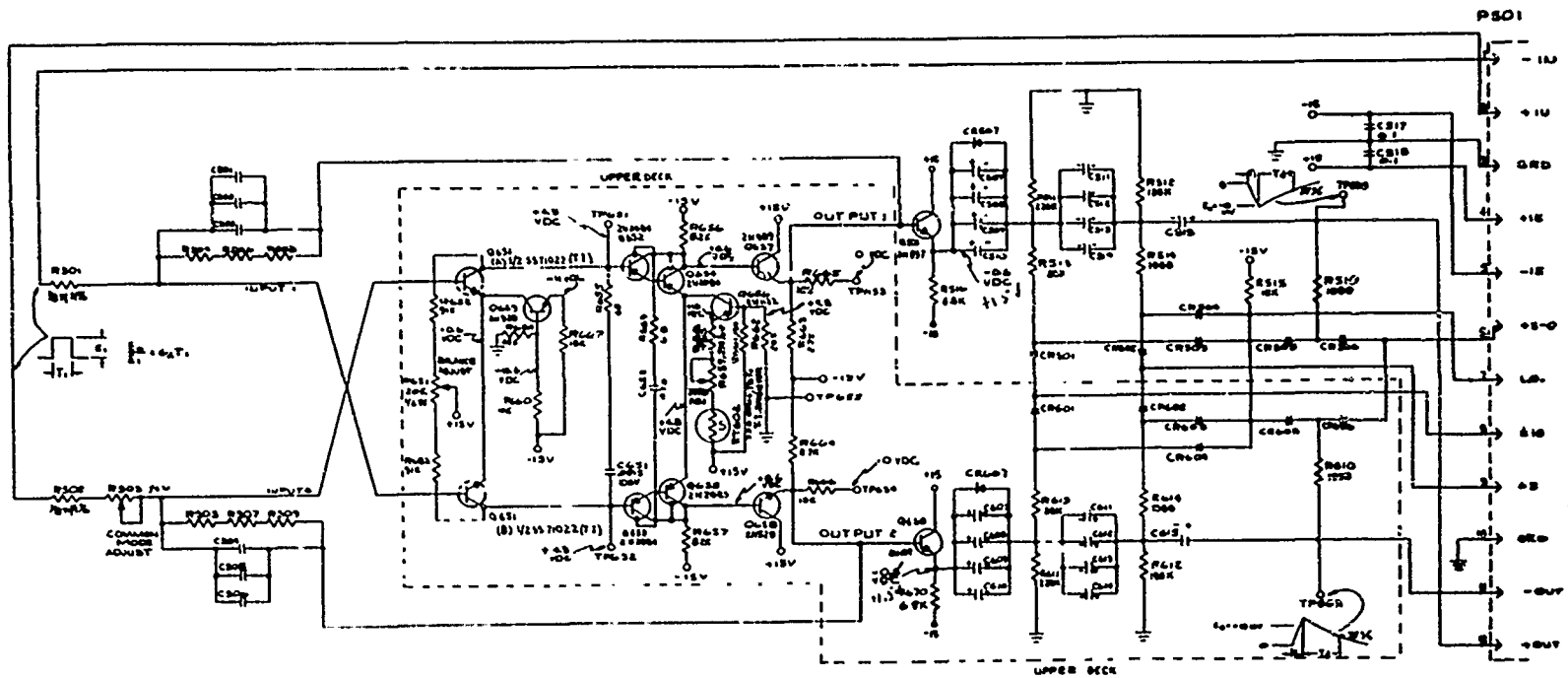

Figure 2.10 Rixon integrator schematic.

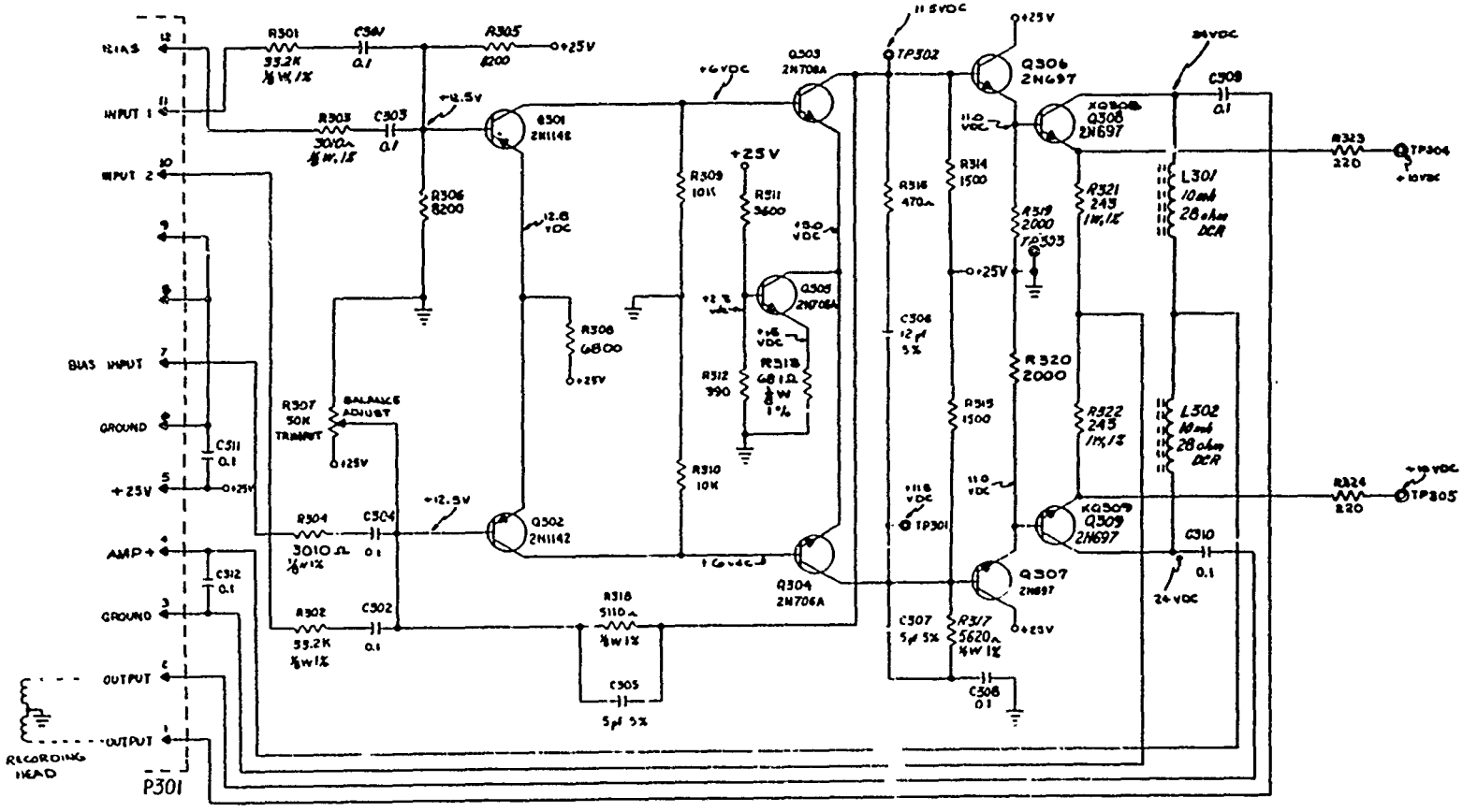

Figure 2.11 Record amplifier schematic.

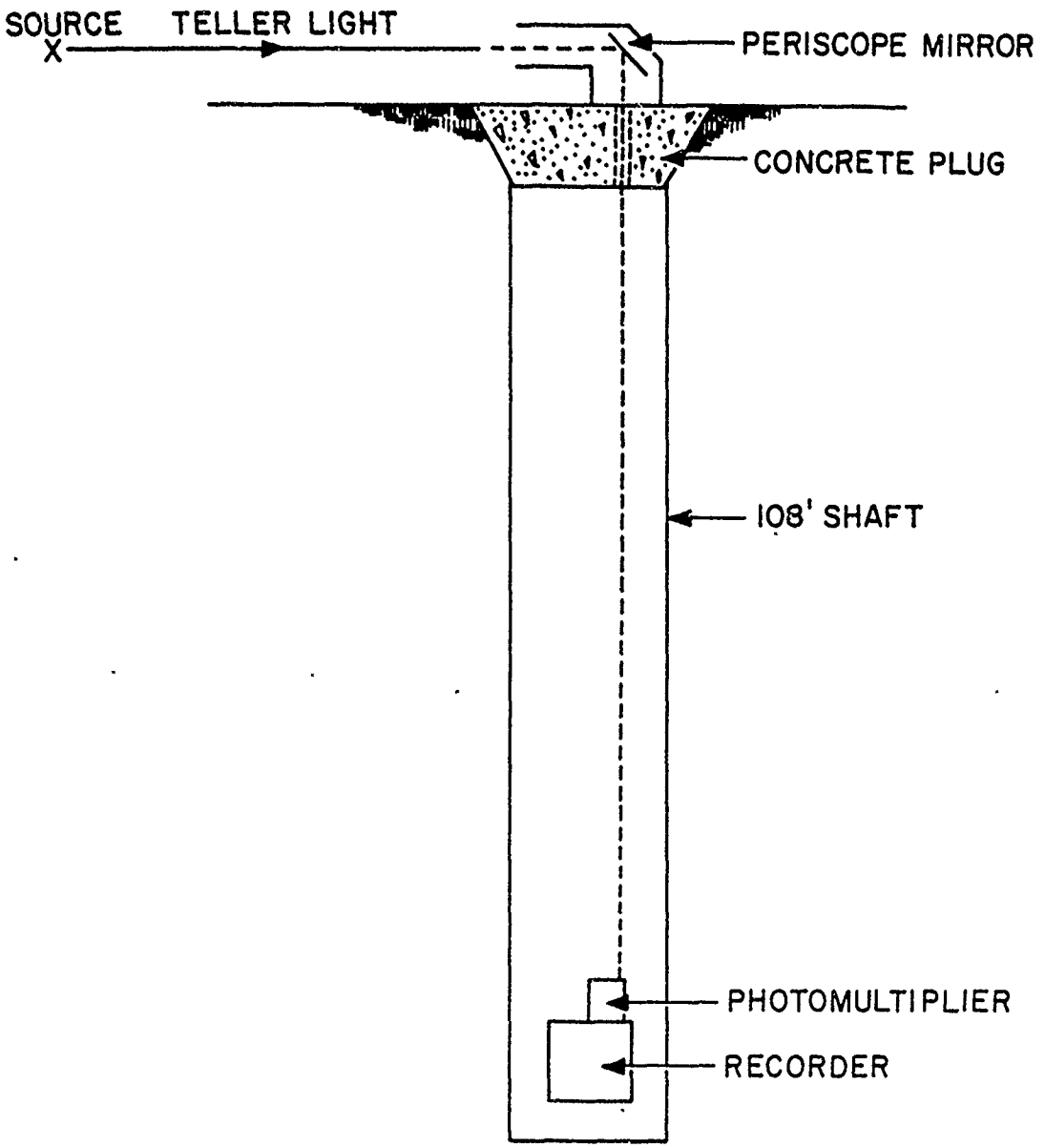

Figure 2.12 Teller light fiducial marker.

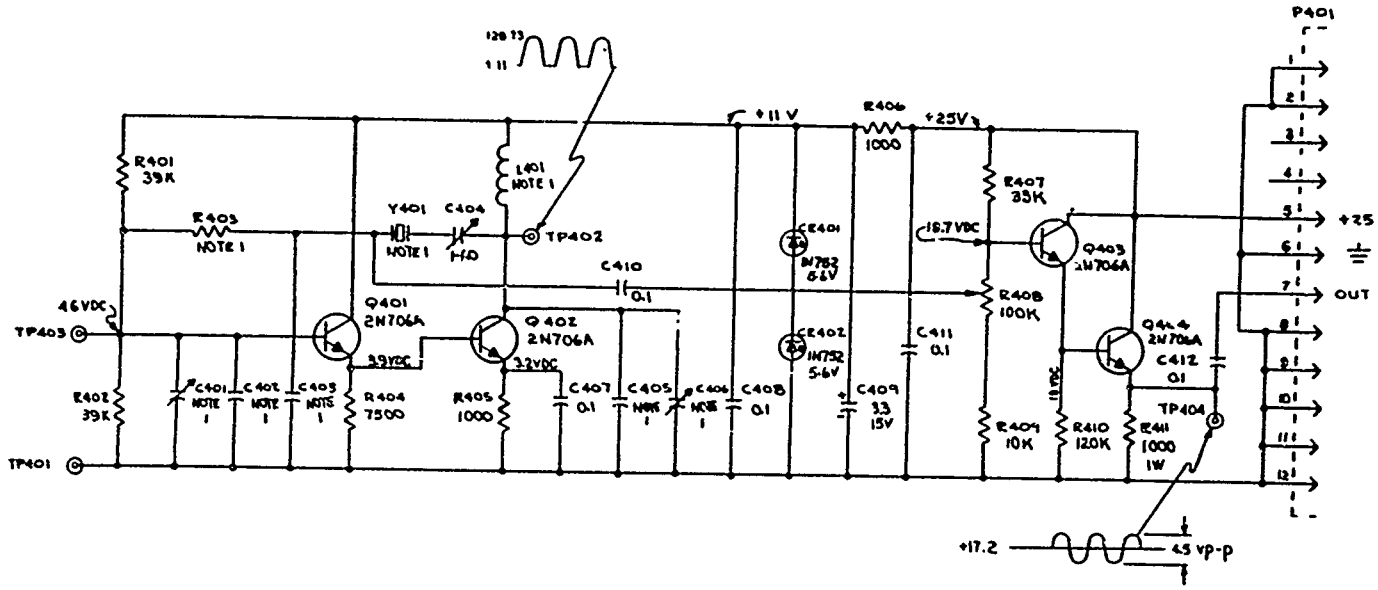

Figure 2.13 Timing oscillator schematic.

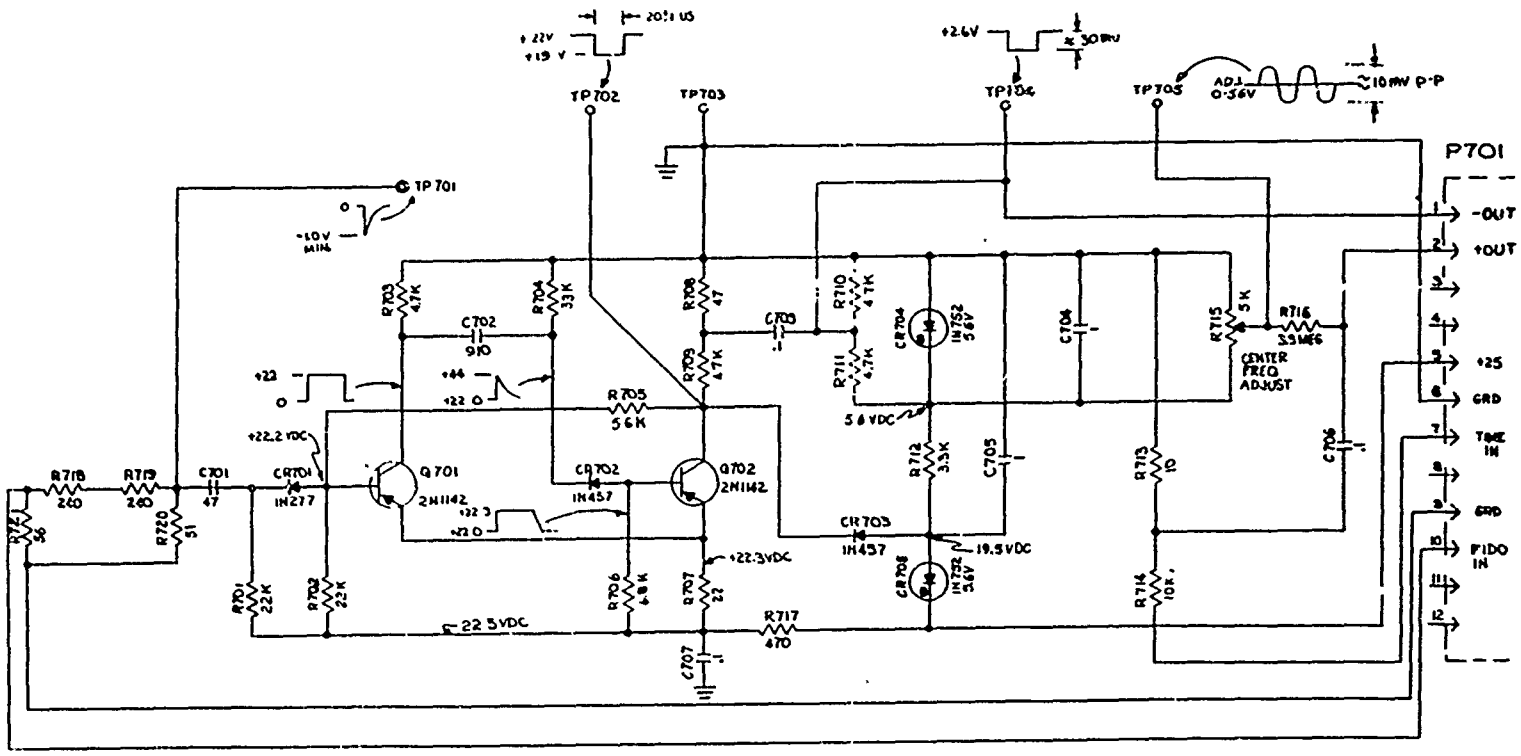

Figure 2.14 Fiducial mixer schematic.

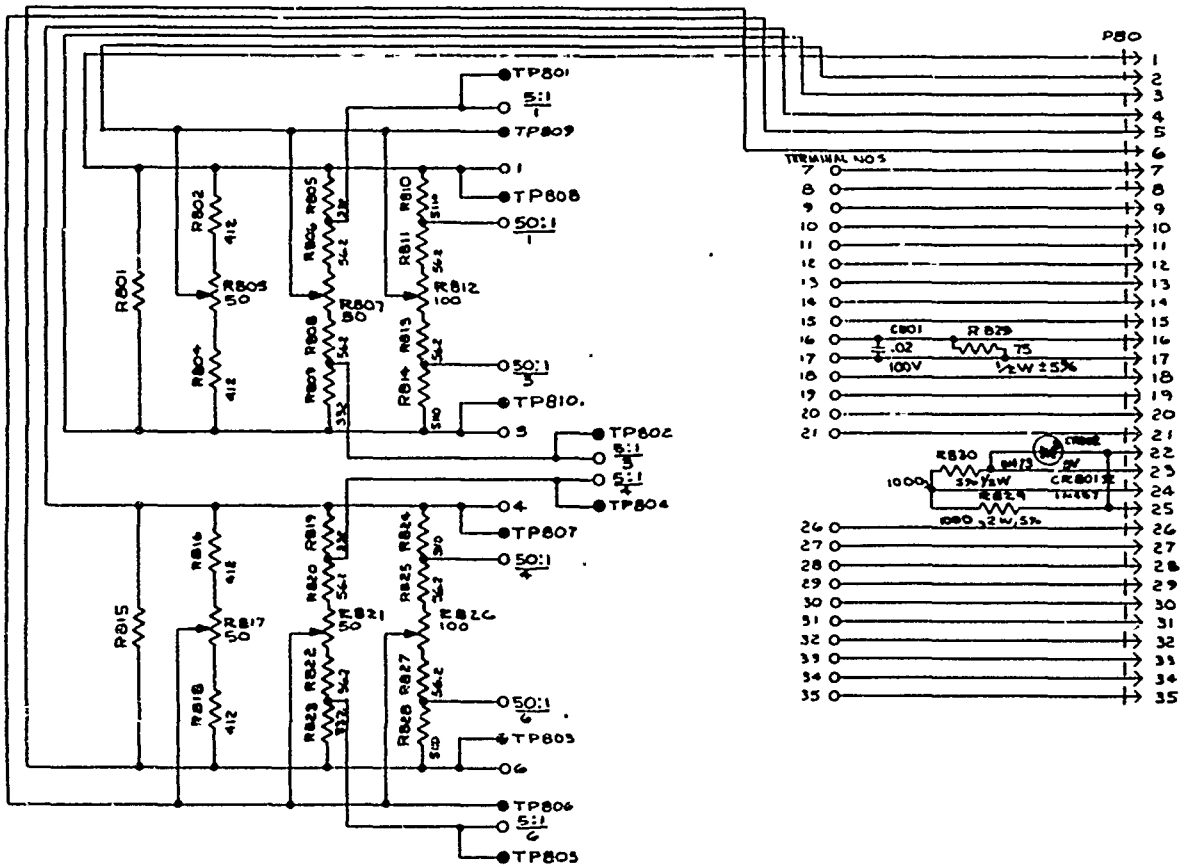

Figure 2.15 Patch card schematic.

CHAPTER 3

RESULTS

3.1 DATA ANALYSIS

Examination of the oscillographic traces showed, in many cases, two disturbing phenomena.

The first type was a large highly damped oscillatory phase starting at the beginning of the trace and lasting on the order of tens of microseconds. The frequency of this oscillation was about 300 kilocycles per second, the upper frequency limit of the integrator-voltage-controlled oscillator-recorder system. Subsequent laboratory analysis indicated that the source of this oscillation was instabilities in the integrator and that the amplitude of this phase was non-linearly dependent on the rate of rise of the input voltage. Unfortunately, on many channels these oscillations were large enough to saturate the succeeding voltage-controlled oscillator for about 10 microseconds so that little useful data could be salvaged.

The second observed phenomena was an apparent constant or very-low-frequency component of the magnetic field at the end of the trace. At the present time, it is believed that this effect is the result of non-linear integration of the large, highly damped ringing that is superimposed on the real signal at the start of the record. The result is a finite and constant error at the end of the ringing phase. Thus, when the real signal has returned to zero value,

the integrator will still have a charge which will leak off with its characteristic decay time. Experiments have corroborated this and have shown that the error is equal to the offset at the start of the integrator decay phase. This, in effect, shifts the zero or base line of the record to this offset point (see Figure 3.1).

This offset point was determined for each record by visual inspection or by extrapolation of the integrator decay phase. The magnetic field time history was then determined by reading many points from the photographic oscillograph of the tape-recorder playback and correcting them by the amount of the offset. The final curves shown are composites of data taken from a number of channels of differing sensitivities. Only self-consistent data were used. Figures 3.2 through 3.28 show the results of this procedure.

3.2 DATA

Data were successfully recovered from all stations except Station 519.03 at 1,600 feet and Station 519.04 at 1,650 feet. At Station 519.03, the tape puller drive belt broke some time during the first 10 seconds before zero time and hence no data were recorded. Unfortunately, the antenna 20 feet above the earth's surface was at this station and this interesting piece of information was not obtained. At Station 519.04, the magnetic tape broke before zero time and no information was recorded. However, there were no magnetic field sensors at this station.

3.2.1 Azimuthal Field. In the following discussion of the data, the time regimes suggested by Dr. C. Longmire of Los Alamos Scientific Laboratory will be used (Reference 6). The first is the wave or exponential phase. During this period the conduction currents, in the air surrounding the detonation point, are small compared to the displacement currents. For all cases of interest the time of this phase is less than a microsecond. The second period is the diffusion phase during which time the conduction currents are larger than the displacement currents but where the skin depth in the air is less than a gamma ray absorption length or the distance of the point of interest from the burst. This phase starts at the end of the wave phase and lasts about 10 microseconds. The third and final phase is the semistatic phase in which the skin depth is a maximum and Compton currents and return currents are approximately in static balance.

The direction of the measured azimuthal field, at all stations, was clockwise around the detonation point. For radial distances up to 1,600 feet, the pulse was unidirectional (see Figures 3.2 through Figure 3.6). At the 4,000-foot station, the oscillatory characteristics of the radiated fields start to make their appearance and at 9,800 feet the wave shape is quite similar to the radiated fields measured at long distances. For example, at Station 519.07 the measured first crossover time is about 14

microseconds (see Figure 3.9). This is in good agreement with electric field measurements made at 12.2 kilometers by Denver Research Institute in Project 6.9 (Reference 7).

It is instructive to compare the shape of the gamma ray flux as a function of time with the magnetic field time history at the same radial distance for close-in stations. Figure 3.11 shows the radiation detector current as a function of time at the 625-foot stations, 519.02 and 519.09. These measurements were made by P. Caldwell in Project 2.1 (Reference 8) at Station 519.02 on the same recorder as the magnetic field measurements. As can be seen, the agreement of shape is quite good. Figure 3.12 shows the same quantities as measured at the 1,600-foot stations, 519.08 and 519.10. The gamma ray measurements were made at the 1,600-foot bunkers used by Projects 2.1, 6.1, and 6.3. The radiation detector current shown is a composite of data recorded on photographic oscillographs directly from oscilloscopes and data recorded on a tape recorder, in the bunker, which was similar to those used to record magnetic field data. The agreement in shape is again quite good, even to agreement in the slight plateau at 80 microseconds. A close relationship between the magnetic field and the local radiation field at least for times greater than about 10 microseconds is thus indicated.

Although there are no peak values shown, at most stations, it is possible to estimate their magnitude. Due to the limited

bandwidth of the recording system, no information during the wave phase could have been faithfully recorded, hence, only the diffusion and semistatic phases are of interest. An estimate of the peak of the diffusion phase at Station 519.01 can be made from an equation given by Longmire (Reference 6) similar to the one on Page 11.

$$H_{\phi} \approx 136 \left[\frac{Ye^{-\frac{R}{\lambda}}}{R^2}\right]^{0.55} \quad \text{ampere turns/meter}$$

where Y is the yield in kilotons

R radial distance in kilometers

λ is the gamma mean free path 0.30 kilometers

$H_{\phi} \cong$ ampere turns/meter

At the 625-foot stations, 519.02 and 519.09, the 1,600-foot station, 519.10, and the 4,000-foot stations, 519.06 and 519.11, estimates of the diffusion phase can be made from calculations of the magnetic field from measured radial electric field, performed by Dr. J. Malik of Los Alamos Scientific Laboratory (Reference 9). At 625 feet, the peak of the diffusion phase is estimated to be about

At 1,600 feet,

and at 4,000 feet, approximately

From the apparent radial field measurements at Station 519.11, the azimuthal field is estimated to be about

Figure 3.10 shows the azimuthal magnetic field measured at Station 519.05 at a radial distance of 1,600 feet and 100 feet in the ground. The shape and amplitude of this pulse agrees quite well with calculations made by Malik (Reference 9) and Fisher (Reference 10) of the magnetic field at a depth of 100 feet in Nevada type soil due to an essentially impulse radial electric field at the surface.

3.2.2 Vertical and Radial Fields. Figures 3.13 to 3.21 show the apparent vertical magnetic fields and Figures 3.22 to 3.28

show the apparent radial fields. As has been mentioned earlier, the apparent fields which are indicated by the vertical and radial antennas, at times less than 1 millisecond, may be the result of local inhomogeneities in soil conductivity which will distort local fields. Thus the amplitude and direction will tend to be random and unpredictable.

Apparent vertical and radial signals can also result from misalignment of these antennas. Thus if, for example, a radial antenna is not precisely orthogonally oriented with respect to the azimuthal field, a voltage will be induced in the radial antenna due to the time derivative of the component of the azimuthal field which is perpendicular to the radial antenna. If θ is the angle between the plane of the loop as it is actually placed and the desired position of the plane, then the maximum voltage induced in either a vertical or radial antenna, due to the azimuthal field, will be equal to $H_\phi \sin\theta$ where H_ϕ is the magnitude of the azimuthal field. It can be seen that if θ is equal to about 2 degrees, which is the estimated alignment error for most stations, the apparent radial field would be about 3 percent of the azimuthal field. In all cases, except three, the measured vertical or radial fields, at times less than 1 millisecond, were approximately equal to or less than 3 percent of the corresponding azimuthal field. It is impossible, at this time, to determine whether the apparent non-azimuthal fields are real, the result of local azimuthal field distortion, or due to antenna misalignment. The latter two explanations seem the most likely.

There is, however, one exception and that is the vertical signal at Station 519.01 (see Figure 3.13). The portion of the signal prior to shock arrival at 0.019 second is still unexplained; however, it is the portion of the signal after this time that is of interest.

Karzas and Latter (Reference 11) have suggested that, close to a nuclear explosion, the earth's magnetic field lines become

frozen into the highly conducting ionized region surrounding the detonation and are carried along with the blast wave or with the slower moving bomb debris as suggested by J. Malik (Reference 12). The field outside the ionized region is unable to penetrate it and is pushed outward. Thus, at a given radial distance, it might be expected that prior to shock arrival there might be a slight increase in ambient field, due to the approaching shock wave piling up the field in front of it, followed by a decrease in magnetic field to below ambient as the shock and debris pass, then followed by a decay back to normal. According to Karzas and Latter, this decay time is determined by such phenomena as fireball rise, and radiative and convective cooling, with times of the order of seconds.

Figure 3.13 shows this behavior quite clearly. In this figure, a negative going signal is equivalent to an increase in the vertical component of the earth's magnetic field; a positive signal is equivalent to a decrease in earth's field. The ordinate, then, represents the change in the earth's field.

The increase of earth's magnetic field can be seen prior to shock arrival at 0.019 second due to the piling up of field. The pile-up decreases as the shock wave and slower moving debris pass. The shock moves as $t^{2/5}$ while the debris moves as $t^{1/3}$. It is to be noted that, at the maximum decrease in field, the earth's field is almost entirely cancelled.

3.2.3 Shock Arrival Measurements. In those figures where shock arrival is indicated, it is to be noted that these recorded signals are due to the rotation of the antenna, caused by the passing shock wave, in the earth's magnetic field. The measured arrival times agree quite well with airblast measurements made in Project 1.1 (Reference 13).

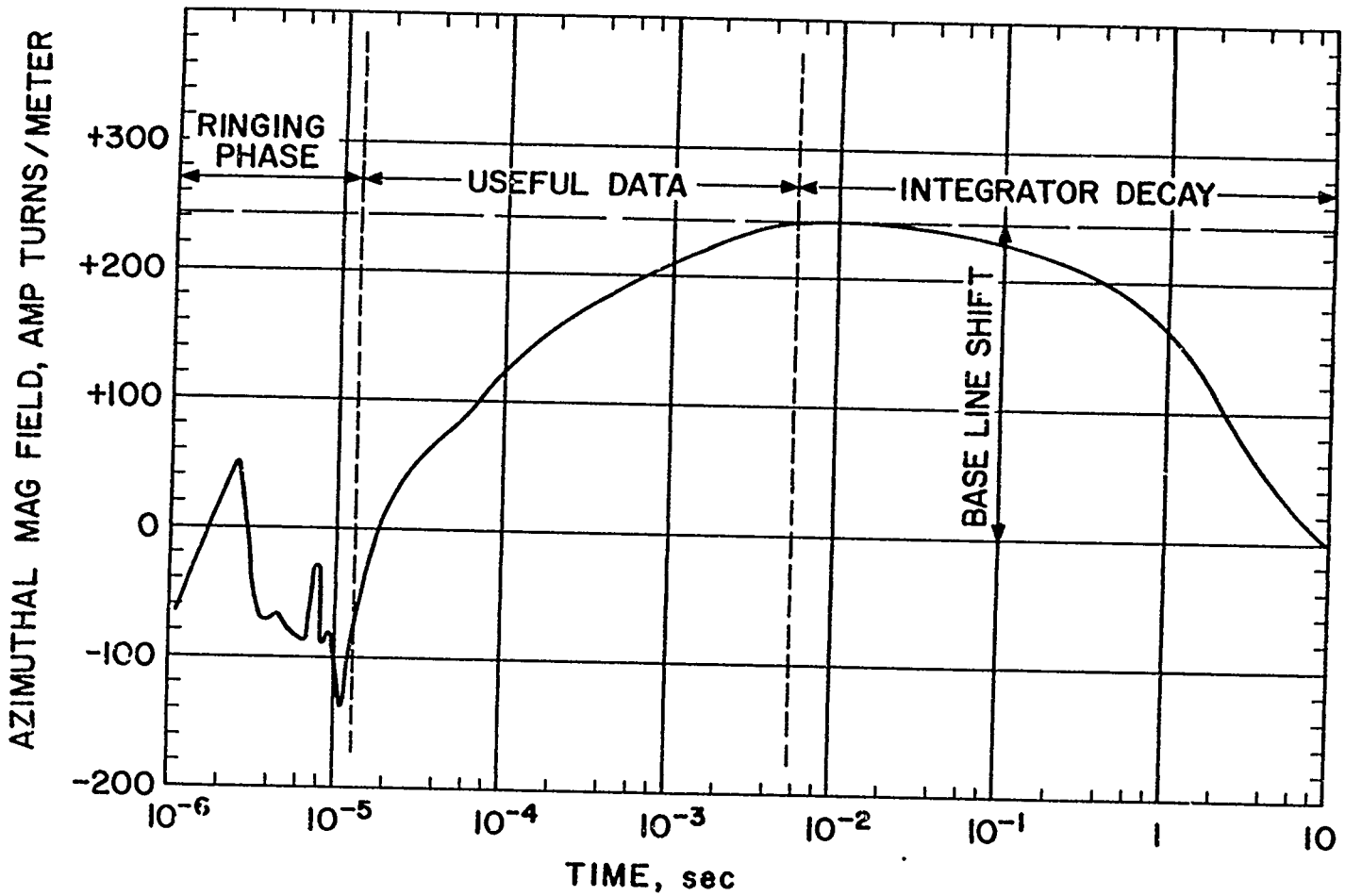

Figure 3.1 Typical uncorrected magnetic field oscillograph.

pages 88 through 114 are deleted

CHAPTER 4

CONCLUSIONS AND RECOMMENDATIONS

In general, the experiment was quite successful. The surface magnetic field was determined to be essentially azimuthal in a clockwise direction around the detonation point. The magnitudes of the measured fields are corroborated by present theories and are consistent with measurements made by other projects. The measurements at 100-foot depth were successful and since information regarding the source is lost by the field in passing through the earth, it seems doubtful if any further measurements deep in the ground need be made. Due to the failure to get information of the field above the surface, it is recommended that this measurement be repeated.

Even though there were data lost at many stations due to instabilities in the integrator used, which can be corrected in the future, the method of integrating the output of a loop antenna is still a very useful one for times greater than about 1 microsecond. Useful as this method may be, for future tests, it is recommended that the search for high frequency, 100-megacycle-response sensors, capable of measuring large magnetic fields directly, be vigorously pursued.

REFERENCES

1. P. H. Haas and others; "Measurement of the Magnetic Field Near a Nuclear Detonation"; Project 6.2, Operation Plumbbob, WT-1436, May 1962; Diamond Ordnance Fuze Laboratories, Washington, D. C.; Secret.

2. "Small Boy Pretest Analysis (U)"; Planning Report No. 1; Research Directorate, Air Force Special Weapons Center, Kirtland Air Force Base, New Mexico; Secret Restricted Data.

3. Dr. Charles A. Blank; "Electromagnetic Pulse Bibliography"; DASA-618, 12 January 1963; Defense Atomic Support Agency, Washington, D. C.

4. George A. Ausman, Jr.; "Field Distribution at the Mid-Plane of a Helmholtz Coil"; Internal Memorandum Report M-230-63-4, 12 August 1963; Harry Diamond Laboratories, Washington, D. C.

5. R. E. Burgess; "The Screened Loop Aerial"; The Wireless Engineer, October 1939, pp 492 to 499.

6. Dr. Conrad Longmire; Los Alamos Scientific Laboratory, Los Alamos, New Mexico; Private communication and lecture notes; Secret Restricted Data.

7. H. Reno; "Correlation of Present and Previous Electric Field Measurements"; Project 6.9, Operation Sun Beam, POR-2234, May 1963; Denver Research Institute, University of Denver, Denver, Colorado; Secret Restricted Data.

8. P. Caldwell and others; "Initial Radiation Measurements"; Project 2.1, Operation Sun Beam, POR-2209; Waterways Experiment Station, Vicksburg, Mississippi; Secret Restricted Data.

9. Dr. John Malik; Memorandums J-13-459, Unclassified, and J-13-460, Secret Restricted Data, 16 March 1964; Los Alamos Scientific Laboratory, Los Alamos, New Mexico.

10. P. F. Fisher; "Underground Magnetic Field Signals from a Near-Surface Burst"; RM 63 TMP-33, DASA-1408, August 1963; GE TEMPO Company, Santa Barbara, California; Secret Formerly Restricted Data.

11. W. J. Karzas and R. Latter; "The Electromagnetic Signal Due to the Exclusion of the Earth's Magnetic Field by Nuclear Explosions"; RAND Corporation Memorandum RM 2890-PR, December 1961; Unclassified.

12. J. Malik; Private communication.

13. J. H. Keefer; "Nuclear Airblast Phenomena"; Project 1.1, Operation Sun Beam, POR-2200, January 1964; Ballistic Research Laboratories, Aberdeen Proving Ground, Maryland; Confidential Formerly Restricted Data.

page 117 is deleted